

Fully Tunable Fano Resonances in Chiral Electronic Transport

Ai-Ying Ye and Zhao Yang Zeng*

Department of Physics, Jiangxi Normal University, Nanchang 330022, China

Fano resonance is believed to arise when a direct path interferes with a resonant path. We demonstrate that this is not true for chiral electronic transmission without additional direct paths. To address the Fano effect in chiral electronic transport, we suggest an electronic Mach-Zehnder-Fano interferometer, which integrates a quantum dot into an electronic Mach-Zehnder interferometer. Due to the absence of backscattering in chiral electronic transport, Fano resonances can be fully adjusted by an external magnetic flux in the transmission, linear conductance, differential conductance and differential shot noise of chiral electrons. Even the current and shot noise for a symmetric interferometer with two arms of the same length exhibit fully controllable resonances and distinct Fano characteristics. In particular, all the profiles in the various transport spectra follow the same evolution pattern in an evolution cycle that is resistant to changes in the device's defining parameters.

I. INTRODUCTION

Fano resonance[1–3], characterized by asymmetric line profiles, is of fundamental and practical interest. It results from interference between one resonant path and one nonresonant (direct) path. The Fano profile is defined as $(\delta + q)^2/(\delta^2 + 1)$, where δ represents the dimensionless detuning and q is the asymmetry parameter. Fano line profiles have been observed in the characteristic spectra of a number of systems, including photoabsorption in atoms[4], neutrons[5] and electrons[6] scattering, Raman scattering[7], photoabsorption in quantum wells[8], scanning tunneling microscopy[9], and conductance through quantum dots (QDs)[10].

Resonant tunneling through QD devices has drawn a great deal of attention in the past decades. Conductance peaks in QDs exhibit the standard Lorentzian profile of a Breit-Wigner resonance $1/(\delta^2 + 1)$ [11, 12], despite strong electron-electron interactions in QDs. One may expect Fano-type line shapes in the transmission through a quantum wire side-coupled to a localized resonant mode[13–16]. The first surprising discovery of the asymmetric line shape of differential conductance occurred in the study of Kondo resonance for tunneling into a surface magnetic atom [9]. Göres et al.[10] conducted a systematic experimental study on the Fano effect in electronic transport through a QD, an electron droplet generated in a two-dimensional electron gas by electrostatic gating, which permits adjusting of resonant width. However, the transition of the conductance dip into a peak by altering the magnetic field is not well understood, and the origin of the nonresonant route is unclear[10, 17]. This work sparked subsequent investigations on Fano resonances in the conductances through an Aharonov-Bohm(AB)ring with a QD embedded in one arm[18–20] and a quantum wire with a side-coupled QD[21–23] in the Coulomb blockade regime, as well as in the Kondo regime[24–29].

There has been little investigation into Fano resonances in chiral electronic transport thus far. Backscattering is entirely suppressed for chiral electrons, and as a consequence, it is meaningless to embed a QD in a chiral quantum wire. Transmission probability through a chiral channel with a side-coupled resonant mode is always unity, irrespective of the electron's incident energy, and thus no Fano resonance can be expected. It is in striking contrast to the nonchiral case where the transmission probability develops a Fano dip at resonance [15, 26, 27, 29] due to resonant reflection. However, if we introduce another chiral mode and allow electrons to tunnel into it, electrons will have two paths to choose from, and interference between these two channels could result in an unexpected Fano effect. To achieve this goal, we assemble the aforementioned elements into an electronic Mach-Zehnder-Fano interferometer (MZFI), which may be the most straightforward configuration to examine the Fano effect in chiral electron transport. The fact that each chiral electron only travels through the interferometer once simplifies the theoretical analysis and unravels the underlying physics more clearly than any nonchiral interferometer, where electrons traverse forth and back many times before departing.

The rest of the paper is organized as follows. In Sec. II, we describe the model of a MZFI connected to four metallic contacts acting as electron sources and drains, formulate it in Hamiltonian language and present an explicit expression to calculate the current flowing into a drain contact. Sec. III is devoted to the analysis of Fano resonances in various transport spectra, including transmission, linear conductance, differential conductance, current, shot noise and differential shot noise. Surprisingly, all the transport spectra of a symmetric MZFI exhibit fully tunable Fano resonances and perform the same evolution pattern within a period as a function of the external magnetic flux. The effect of asymmetry in the lengths of two arms of the interferometer and interacting QD in the Coulomb blockade and Kondo regime is analyzed and elucidated in Sec. IV. We argue that, not being perfect, Fano resonances still persist and are fully tunable under these circumstances. Concluding remarks and possible

* zyzeng@hunnu.edu.cn

further investigations in the chiral Fano effect are given in Sec. V.

The calculations in this work were tedious and quite involved. We have relegated many of the details to four appendixes. In Appendix A we present a detailed derivation of the current flowing into a drain contact in the absence of contact Hamiltonian using the equation-of-motion method and the Keldysh equation. A standard Keldysh formalism to recover the current expression in the presence of contact Hamiltonian is presented as a complementary in Appendix B. In Appendix C we justify the assumption $\theta(0) = 1/2$ made in Appendix A 3 from the scattering matrix approach. Scattering matrix and shot noise of the device are derived based on the Fisher-Lee relation[53, 54] in Appendix D.

II. MODEL AND FORMULATION

We consider a four-terminal electronic Mach-Zehnder-Fano interferometer (MZFI), a device schematically sketched in Fig. 1 that integrates a QD into an electronic Mach-Zehnder interferometer (MZI)[30–43]. An electronic MZFI in a quantum Hall liquid at filling factor $\nu = 1$ can be realized through the deposit of elaborately-tailored split metallic gates on the surface of the involved semiconductor heterostructure[30, 33, 39]. Two inner edge states are employed as the chiral modes propagating along the two arms of the interferometer. Ohmic contacts serve as carrier sources (S_1, S_2), each injecting a carrier stream split at x_1 by the first quantum point contact (QPC1) to two partial beams. One moves along the upper arm with a nearby QD at x_d , which provides the resonant path in the Fano model, while the other moves down the lower arm. They recombine at x_2 by the second quantum point contact (QPC2) and interfere, resulting in two complementary currents that are collected by another two ohmic contacts functioning as drains (D_1, D_2).

The Hamiltonian describing such a device is $H_D = \sum_{\alpha=u,l} H_\alpha + H_d + H_{ul} + H_{ud}$. While H_d and H_{ud} explain the localized mode in the QD and coupling between the QD and the upper edge, H_α and H_{ul} reflect the free motion along each edge and interedge electron tunneling. In terms of field operator annihilating an electron at position x on the edge α , $\hat{\psi}_\alpha(x)$, the Hamiltonian of free chiral modes is defined as follows: $H_\alpha = -i\hbar v_F \int dx \hat{\psi}_\alpha^\dagger(x) [\partial_x + ieA_\alpha(x)/\hbar c] \hat{\psi}_\alpha(x)$, where v_F is the Fermi velocity and $A_\alpha(x)$ is the magnetic vector potential experienced by chiral electrons on the edge α at position x . The interedge tunneling Hamiltonian is written as $H_{ul} = \sum_{j=1,2} [t_j \hat{\psi}_u^\dagger(x_j) \hat{\psi}_l(x_j) + H.c.]$, where the tunneling amplitude is $t_j = 2\hbar v_F \gamma_j$ and $H.c.$ denotes Hermitian conjugate. This indicates that electrons can be reflected or transmitted at the positions x_1 and x_2 of the two QPCs. The QD consists of non-interacting levels ϵ_i with localized modes $\xi_i(x)$. It is assumed that the level spacing of the QD $\Delta\epsilon_i \propto 1/L_d$ is comparably large as long as the circumference L_d of the dot is small enough. In this case,

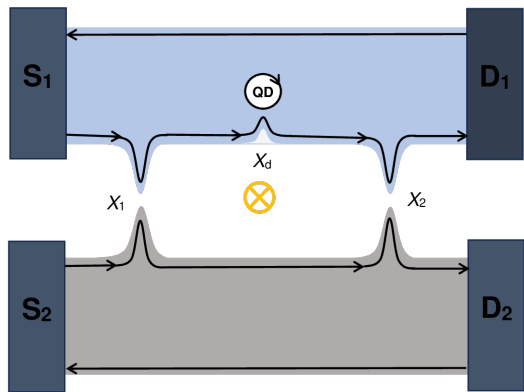


FIG. 1. Schematic illustration of a four-terminal electronic MZFI: Two chiral edge states, represented by arrowhead lines, are formed at the boundaries of two quantum Hall fluids of opposite chirality (light blue and light grey regions) at filling factor $\nu = 1$. A QD is etched close to the inner edge of a fluid, enabling electrons to tunnel between the edge and the dot, thus providing the resonant path in the Fano model. QPC1 splits the incoming electron beam from S_1 or S_2 into two portions propagating along the upper and lower arms; QPC2 recombines two portions back together, with resultant outgoing currents collected and measured at D_1 and D_2 . The two arms encircle a magnetic flux Φ and form an AB ring.

tunneling via only one discrete state is prominent if the energy ϵ_d of this state $\xi_d(x)$ is close to the Fermi energy of the upper edge. To describe tunneling between the QD and the upper edge, we express the QD field in terms of annihilation operators $\hat{\psi}_d(x) = \hat{d}\xi_d(x) + \sum_i \hat{d}_i \xi_i(x)$. The effective tunneling Hamiltonian H_{ud} is given by substituting the QD field in the projected subspace $\xi_d(x)$ into the bare tunneling term $[t_{du} \hat{\psi}_u^\dagger(x_d) \hat{\psi}_d(x_d) + H.c.]$: $H_{ud} = [t_d \hat{\psi}_u^\dagger(x_d) \hat{d} + H.c.]$, where the tunneling amplitude $t_d = t_{ud} \xi(x_d) = \sqrt{2\hbar v_F \gamma_d} / \sqrt{a}$ with a the characteristic length of the contact. In this projected subspace, the QD may be modelled by the Hamiltonian $H_d = \epsilon_d \hat{d}^\dagger \hat{d}$. Under the gauge transformation $\hat{\psi}_\alpha(x) \rightarrow e^{\frac{ie}{\hbar c} \int_{x_0}^x dx A_\alpha(x)} \hat{\psi}_\alpha(x)$, $A_\alpha(x)$ -dependence is removed from the free edge Hamiltonian, while the tunneling amplitudes t_j is replaced by $t_j e^{\frac{ie}{\hbar c} [\int_{x_0}^{x_j} dx A_u(x) - \int_{x_0}^{x_j} dx A_l(x)]}$.

The MZFI is assumed to be coupled ballistically to four contacts at various electrochemical potentials $\mu_{i\alpha}$ via leads, where the upper or lower edge is denoted by $\alpha = u, l$ (or 1, 2) and the source or drain is labeled by $i = S, D$. Chiral electrons are assumed to propagate rightward from source to drain. The continuity equation $\partial_t \hat{\rho}_\alpha^e + \partial_x \hat{I}_\alpha = 0$ ($\alpha = u, l$) may be used to read the current $I_\alpha(x)$ flowing along edge α , where $\hat{\rho}_\alpha^e(x, t) = -e \hat{\psi}_\alpha^\dagger(x, t) \hat{\psi}_\alpha(x, t)$ is the chiral electron density operator on the edge α . The Heisenberg equation of motion for $\hat{\rho}_\alpha^e(x, t)$ yields $\partial_t \hat{\rho}_\alpha^e(x, t) = [\hat{\rho}_\alpha^e(x, t), H_D] / i\hbar = -v_F \partial_x \hat{\rho}_\alpha^e(x, t)$. Hence one finds

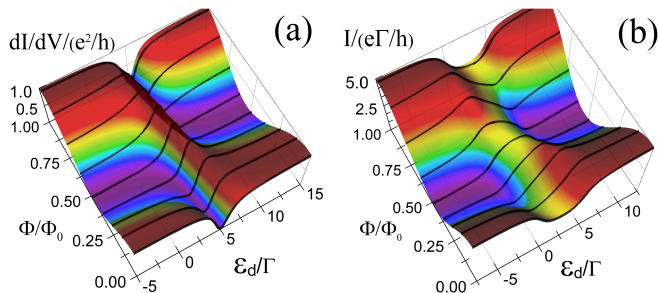


FIG. 2. Differential conductance dI/dV in units of e^2/h (a, left panel) and current I in units of $e\Gamma/h$ (b, right panel) at zero temperature are plotted as functions of the dot level ϵ_d/Γ with varying magnetic flux Φ/Φ_0 . The parameters are: $T_1 = T_2 = 0.5$, $eV = 5\Gamma$.

$$\begin{aligned} I_\alpha(x) &= v_F \langle \rho_\alpha^e(x, t) \rangle_{H_D} = i e \hbar v_F G_{\alpha\alpha}^<(x, t; x, t) \\ &= \frac{e}{\hbar} \int d\epsilon i \hbar v_F G_{\alpha\alpha}^<(x, x; \epsilon), \end{aligned} \quad (1)$$

where $G_{\alpha\alpha}^<(x, t; x', t') = i \langle \hat{\psi}_\alpha^\dagger(x', t') \hat{\psi}_\alpha(x, t) \rangle_{H_D} / \hbar$ is the lesser Green's function of the edge α . $I_\alpha(x)$, when evaluated at a position x in lead D_i , represents the current I_{D_i} detected in drain i following the notation $i = 1$ if $\alpha = u$ and $i = 2$ if $\alpha = l$, since the device is assumed to be connected ballistically to the leads.

We calculate the current I_{D_1} transmitted into drain 1, using the equation-of-motion method in real space and the Keldysh technique (for details, See the Appendixes A and B), and find

$$I_{D_1} = I_{D_1}^0 + \frac{e}{\hbar} \int_{-\infty}^{+\infty} d\epsilon [f_{S_2}(\epsilon) - f_{S_1}(\epsilon)] \mathcal{T}_{D_1 S_2}(\epsilon), \quad (2)$$

where

$$I_{D_1}^0 = \frac{e}{\hbar} \int_{-\infty}^{+\infty} d\epsilon [f_{D_1}(\epsilon) - f_{S_1}(\epsilon)] \quad (3)$$

is the direct current transmitted from S_1 into D_1 without interedge and edge-dot tunnelings, and

$$\mathcal{T}_{D_1 S_2}(\epsilon) = |\sqrt{R_1 T_2} + \sqrt{T_1 R_2} \tau_d(\epsilon) e^{-i\phi}|^2 \quad (4)$$

is the transmission probability from lead S_2 to lead D_1 . Here $T_i = 4\gamma_i^2/(1+\gamma_i^2)^2$ and $R_i = (1-\gamma_i^2)^2/(1+\gamma_i^2)^2$ are the transmission and reflection coefficients of the QPCi, respectively; $\phi = \phi_{AB} + \phi_L$, $\phi_{AB} = 2\pi \frac{\Phi}{\Phi_0}$ is the AB phase with Φ being the magnetic flux enclosed by two arms of the interferometer and $\Phi_0 = hc/e$ the flux quantum, and $\phi_L = \epsilon \Delta L / \hbar v_F$ is the phase shift resulting from the length difference $\Delta L = L_l - L_u$ of the two arms; $\tau_d(\epsilon) = \frac{\epsilon - \epsilon_d - i\Gamma}{\epsilon - \epsilon_d + i\Gamma}$ is the transmission amplitude through the position x_d where the QD is coupled, with $\Gamma = \hbar v_F \gamma_d^2 / d$ the width of the resonant level ϵ_d . It should be noted that, instead of 1, the value of the heaviside

function $\theta(x)$ at zero has been assumed to be 1/2, i.e., $\theta(0) = 1/2$ to obtain the transmission amplitude $\tau_d(\epsilon)$. This assumption is supported within the scattering matrix approach in Appendix C.

Eq. (2) shows that when both edges are coupled to the same source and drain only direct current persists, suggesting that quantization of the Hall conductance is independent of interedge tunneling and impurity scattering. For this reason, we will concentrate on the case in which $\mu_{S_1} = \mu_{D_1} = 0$, $\mu_{S_2} = \mu_{D_2} = eV$ achieved by setting the electrochemical potentials of four contacts in this manner. The current incident from S_2 , denoted by $I = I_{D_1} = \frac{e}{\hbar} \int d\epsilon [f(\epsilon - eV) - f(\epsilon)] \mathcal{T}_{D_1 S_2}(\epsilon)$, is the only nonzero current.

III. ANALYSIS OF FANO RESONANCES

A. Transmission

By defining a background transmission probability without edge-dot tunneling, $\mathcal{T}_{D_1 S_2}^0(\phi) = |\sqrt{R_1 T_2} + \sqrt{T_1 R_2} e^{-i\phi}|^2$, and $\mathcal{A} = \sqrt{T_1 R_1 T_2 R_2}$, the transmission probability can be expressed in terms of a dimensionless detuning $\delta(\epsilon) = (\epsilon - \epsilon_d)/\Gamma$ as

$$\mathcal{T}_{D_1 S_2}(\epsilon) = \mathcal{T}_{D_1 S_2}^0(\phi) - 4\mathcal{A} \frac{\sin\phi\delta(\epsilon) + \cos\phi}{\delta^2(\epsilon) + 1}. \quad (5)$$

Fano resonance is seen in the profile term of Eq. (5), where the antisymmetric part $\delta(\epsilon)/[\delta^2(\epsilon) + 1]$ is represented by a peak at $\delta(\epsilon) = 1$ and a dip at $\delta(\epsilon) = -1$, and the symmetric part $1/[\delta^2(\epsilon) + 1]$ is characterized by a peak of width 2 at $\delta(\epsilon) = 0$. As $\phi = 0$, this transmission probability exhibits a symmetric dip that is unique to the Fano resonance and fits neatly into the Fano profile.

$$\mathcal{T}_{D_1 S_2}(\epsilon) = \mathcal{T}_{D_1 S_2}^0(\pi) + \frac{4\mathcal{A}}{1 + q^2(\phi)} \frac{[\delta(\epsilon) + q(\phi)]^2}{\delta^2(\epsilon) + 1}, \quad (6)$$

where the Fano asymmetry parameter is denoted by $q(\phi) = -\tan(\phi/2)$. Eq. (6) predicts one minimum at $\delta(\epsilon) = -q(\phi)$ and one maximum at $\delta(\epsilon) = 1/q(\phi)$ in the transmission profile. If $q = 0$, there appears a single symmetric peak; if $q \rightarrow \pm\infty$, there appears a single symmetric dip. In terms of the transmission phase $\phi_d(\epsilon) = \arctan[2\delta(\epsilon)/(1 - \delta^2(\epsilon))] - \pi$, the transmission amplitude $\tau_d(\epsilon) = e^{i\phi_d(\epsilon)}$. This leaves us with a well-known expression for the transmission probability $\mathcal{T}_{D_1 S_2} = |\sqrt{R_1 T_2} + \sqrt{T_1 R_2} e^{i[\phi_d(\epsilon) - \phi]}|^2$. Constructive or destructive interference takes place when the phase difference $\phi_d(\epsilon) - \phi$ is 0 or π . The locations of the maxima and minima in the transmission spectrum can be found using the inverse trigonometric identities $2\arctan(x) = \arctan[2x/(1 - x^2)]$, $x^2 < 1$ and $\arctan(x) + \text{arccot}(x) = \pi/2$. These relations are equivalent to the condition of constructive or destructive interference. If we additionally assume a symmetric interferometer, $\Delta L = 0$, the Fano asymmetry parameter

$q = -\tan(\phi_{AB}/2)$ becomes merely a function of the **AB** phase. Consequently, it is possible to fully tune Fano resonances in the transmission and linear conductance spectra of the **MZFI**, simply by tuning the asymmetry parameter with an external magnetic flux.

B. Current and conductance

At zero temperature, the current is given by

$$I = \frac{e\Gamma}{h} \left[\mathcal{T}_{D_1 S_2}^0(\phi_{AB}) \frac{eV}{\Gamma} - 4\mathcal{A} \left[\frac{\sin\phi_{AB}}{2} \ln(\delta^2(\epsilon) + 1) + \cos\phi_{AB} \arctan\delta(\epsilon) \right] \Big|_0^{eV} \right], \quad (7)$$

where $f(\epsilon)|_b^a = f(a) - f(b)$, and the differential conductance is calculated as

$$\frac{dI}{dV} = \frac{e^2}{h} \left[\mathcal{T}_{D_1 S_2}^0(\phi_{AB}) - 4\mathcal{A} \frac{\sin\phi_{AB}\delta(eV) + \cos\phi_{AB}}{\delta^2(eV) + 1} \right], \quad (8)$$

which can be also expressed as $\frac{dI}{dV} = \frac{e^2}{h} \mathcal{T}_{D_1 S_2}(eV)$.

Although their profiles appear to be quite different, the differential conductance and current are the same type of oscillatory function of the **AB** phase with period 2π as the transmission probability, performing identical profile evolution as the **AB** phase grows. However, since the current is the integration of the transmission probability over energy from 0 to eV , their profiles are closely related, and the current profile depends apparently on the applied voltage V . The profile function in Eq. (7) possesses two unusual features: the arctangent term acts as the symmetric component, resulting in a peak at $\epsilon_d = eV/2$ that broadens with rising eV , and the logarithmic term behaves as the antisymmetric part, admitting a dip at $\epsilon_d = eV$ and a peak at $\epsilon_d = 0$. Due to the cumulative effect of integration, the current profiles can be viewed as enlarged versions of the transmission ones.

In actual experiments, it is more convenient to adjust the resonant level ϵ_d by varying the bias voltage to the plunger gate of the dot, with the voltage V being fixed. As functions of the dot level ϵ_d and the enclosed magnetic flux Φ/Φ_0 , we display the differential

$$\frac{dS}{dV} = \frac{2e^3}{h} \left[\mathcal{T}_{D_1 S_2}^0(\phi_{AB}) \mathcal{T}_{D_2 S_2}^0(\phi_{AB}) + 8\mathcal{A}^2 [\cos(2\phi_{AB}) \frac{2\delta^2(eV)}{[\delta^2(eV) + 1]^2} + \sin(2\phi_{AB}) \frac{\delta(eV)[\delta^2(eV) - 1]}{[\delta^2(eV) + 1]^2}] \right], \quad (10)$$

and shot noise

$$S = \frac{e^2\Gamma}{h} \left[\mathcal{T}_{D_1 S_2}^0(\phi_{AB}) \mathcal{T}_{D_2 S_2}^0(\phi_{AB}) \frac{eV}{\Gamma} + 8\mathcal{A}^2 [\cos(2\phi_{AB}) P_S(\epsilon_d, eV) + \sin(2\phi_{AB}) P_A(\epsilon_d, eV)] \right], \quad (11)$$

where $\mathcal{T}_{D_2 S_2}^0$ is defined similar to $\mathcal{T}_{D_1 S_2}^0$, $P_S(\epsilon_d, eV) = [\arctan\delta(\epsilon) - \delta(\epsilon)/[\delta^2(\epsilon) + 1]]|_0^{eV}$ and $P_A(\epsilon_d, eV) =$

conductance in Fig. 2(a) and the current in Fig. 2(b) by setting $eV = 5\Gamma$. These may be clearly seen by taking $T_1 = T_2 = 0.5$. The differential conductance and the current, albeit having different profiles, exhibit fully tunable Fano resonances by adjusting the magnetic flux, as predicted. They also show identical profile progression over the increasing magnetic flux. In contrast to the sharp peak-dip structure in the differential conductance, the accumulation effect causes the peaks and dips in the current spectrum to broaden significantly and appear as arches and valleys, as can be seen in Fig. 2. Observe that for any finite voltage V , the chiral transport is coherent, which is in line with the experimental observation[42] and the theoretical result[35] in the study on decoherence in the electronic **MZIs**. In our configuration, the **QD** is essentially an indispensable component of the coherent transport device as a whole. In contrast to the circumstances [39, 44, 45] where the **QD** functions as a detecting apparatus, it does not cause any dephasing.

C. Shot noise

Due to interference, Fano resonances arise in all the transmission probability through a **MZFI**. Therefore one may expect Fano resonances in shot noise of electronic **MZFIs** as well. At zero temperature, $\Delta I_{S_1} = \Delta I_{S_2} = 0$, there is no noise in the incident stream according to the coherent scattering theory[47–49]. The currents flowing into the drain contacts, I_{D_1} and I_{D_2} , are the only ones that fluctuate. Because of current conservation, $\Delta I_{D_1} + \Delta I_{D_2} = 0$. The transmissions probabilities from lead S_j to lead D_i are associated with the scattering matrix elements of the system by $\mathcal{T}_{D_i S_j} = |s_{D_i S_j}|^2$. Flux conservation yields $\sum_{i=1,2} \mathcal{T}_{D_i S_j} = 1$. As we show in Appendix D, nonzero components of the shot noise power tensor are $S = S_{D_1 D_1} = S_{D_2 D_2} = -S_{D_1 D_2} = -S_{D_2 D_1}$. They are given by (for details, see Appendix D)

$$S = \frac{e^2}{\pi\hbar} \int_0^{eV} d\epsilon \mathcal{T}_{D_1 S_2}(\epsilon) \mathcal{T}_{D_2 S_2}(\epsilon), \quad (9)$$

which gives differential shot noise

$[1/[\delta^2(\epsilon) + 1] + \ln[\delta^2(\epsilon) + 1]/2]|_0^{eV}$ are the symmetric and antisymmetric parts of the profile function of the shot

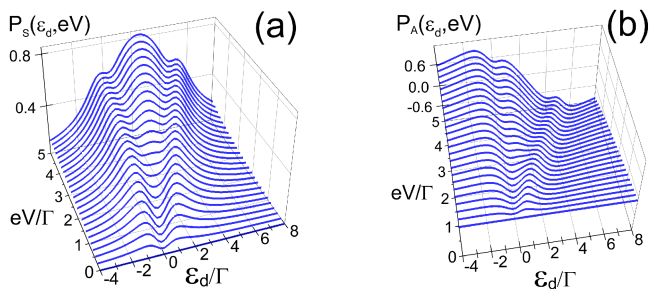


FIG. 3. Evolution of symmetric $P_S(\epsilon, eV)$ (a, left panel) and antisymmetric $P_A(\epsilon, eV)$ (b, right panel) parts of the profile function in shot noise as the voltage eV increases from 0 to 5Γ .

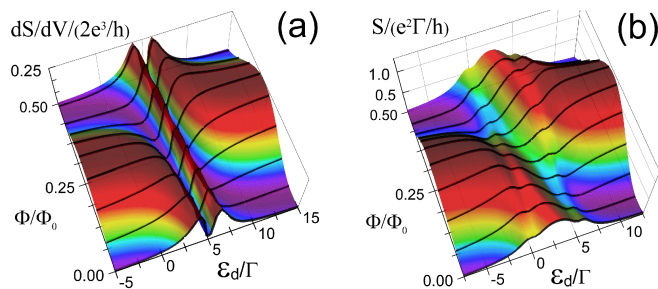


FIG. 4. Differential shot noise dS/dV in units of $2e^3/h$ (a, left panel) and shot noise S in units of $e^2\Gamma/h$ (b, right panel) are plotted as functions of the dot level ϵ_d/Γ with varying magnetic flux Φ/Φ_0 . The parameters are the same as in Fig. 2

noise. As functions of **AB** phase, the differential shot noise and shot noise execute the identical oscillation with halved period π . The ratio of the shot noise to the Poisson noise, $F = S/S_P = S/2eI$, is known as the Fano factor[49]. An equivalent definition of the differential Fano factor may be $F_d = (dS/dV)/2e(dI/dV)$. If the **QD** is removed from the device, these two factors coincide and reduce to $F^0 = F_d^0 = \mathcal{T}_{D_2S_2}^0 = |\sqrt{R_1R_2} - \sqrt{T_1T_2}e^{-i\phi_{AB}}|^2$, which is always no greater than 1 and exhibit **AB** oscillations. Once the **QD** is involved, the Fano factor F evolves in a complicated way, while the differential Fano factor F_d remains rather simple and acquires the form of the transmission $\mathcal{T}_{D_2S_2}(eV)$, thus showing perfect Fano resonances.

The product of two transmission probabilities, $\mathcal{T}_{D_1S_2}(eV)$ and $\mathcal{T}_{D_2S_2}(eV)$, determines the differential shot noise. It takes maximum values when one of them is halfway between its maximum and minimum, and minimum values when either of the two coefficients is maximal or minimal. As a result, the differential shot noise spectrum shows dips where the differential conductance appears as a peak or a dip, and peaks halfway between the ridge and the valley in the differential conductance spectrum. Such an intuitive picture can be verified by examining the profile function of differential shot noise in Eq. (10), which is reminiscent of the line

shape of complex susceptibility of three-level atomic systems in electromagnetically induced transparency (EIT) phenomenon[46]. EIT, or absorption cancellation, is caused by destructive interference between the two coherent routes for absorption and is comparable to Fano antiresonance. The antisymmetric part of the profile in the sine term admits, on the positive side of the $\delta(eV)$ -axis, a sharp dip of depth 0.25 at $\delta(eV) = \sqrt{2} - 1$ and a broad peak of height 0.25 at $\delta(eV) = 1 + \sqrt{2}$. The symmetric part of the profile in the cosine term is peaked symmetrically at $\delta(eV) = \pm 1$ and drops to zero at the midpoint $\delta(eV) = 0$. Depending on ϕ_{AB} , either of these two terms dominates, or both cooperate, resulting in symmetric double-peak or double-dip profiles, or asymmetric profiles with a deformed double-peak or double-dip structure in the differential shot noise spectrum. In the case of shot noise, the symmetric component $P_S(\epsilon, eV)$ has a profile of two or three peaks symmetric about the $\epsilon_d = eV/2$, depending on the ratio of eV/Γ . On the other hand, the antisymmetric component $P_A(\epsilon, eV)$ gives us a profile of a sharp peak with a broad dip on the right and a broad peak on the left as long as $eV < 2\Gamma$. The sharp peak splits and gradually develops into two side shoulders that are located at $\epsilon_d = 0$ and $\epsilon_d = eV$ as eV increases. Figures 3(a) and 3(b) display clearly the evolutions of the symmetric and antisymmetric components of the shot noise profile with increasing voltage eV . We stress that, unique to Fano resonances, a profile of symmetric double-peak with a dip at the center $\epsilon_d = eV/2$ and a profile of symmetric double-peak or triple-peak should be detected in differential shot noise and shot noise spectra of a **MZFI**. We provide profile evolutions of the differential shot noise from Eq. (10) in Fig. 4(a) and shot noise from Eq. (11) in Fig. 4(b), where the magnetic flux Φ/Φ_0 varies from 0 to 0.5. Figures 4(a) and 4(b) confirm our analysis. Furthermore, the evolution pattern in both the differential shot noise and shot noise is identical to that in the differential conductance and current throughout one evolution cycle. Profile evolutions of all the transport spectra of a **MZFI** are determined by sine and cosine functions, therefore, this result comes as no surprise.

IV. DISCUSSION

A. Asymmetric **MZFI**

We have investigated Fano resonances in transport spectra for a symmetric **MZFI** with $\Delta L = 0$. The presence of interferometer arm asymmetry, for example, $\Delta L = L_l - L_u > 0$, will introduce another energy scale $E_A = \hbar v_F/\Delta L$ in the problem. The replacement $\phi_{AB} \rightarrow \phi_{AB} + eV/E_A$ can be used to explain how the asymmetry in interferometer arm lengths affects differential transport spectra including differential conductance, differential shot noise, and differential Fano factor. As for the asymmetry effect on the integrated spectra such

as the current and shot noise, we are interested in the case where there is a small mismatch between the arm lengths such that $E_A \gg eV, \epsilon_d, \Gamma$. The presence of the asymmetry effect is indicated by a slight modification of the symmetric (P_S) and antisymmetric (P_A) parts of the profile functions, so that, up to first order in $1/E_A$, $P'_S \approx (1 - \frac{\Gamma}{E_A})P_S + \frac{\epsilon_d}{E_A}P_A$, $P'_A \approx (1 - \frac{\Gamma}{E_A})P_A - \frac{\epsilon_d}{E_A}P_S$ for current, and $P'_S \approx (1 - \frac{2\Gamma}{E_A})P_S + \frac{2\epsilon_d}{E_A}P_A - \frac{2\Gamma}{E_A}\arctan\delta(\epsilon)|_0^{eV}$, $P'_A \approx (1 - \frac{2\Gamma}{E_A})P_A - \frac{2\epsilon_d}{E_A}P_S - \frac{\Gamma}{E_A}\ln[\delta^2(\epsilon) + 1]|_0^{eV}$ for shot noise. The integrations in the current and shot noise equations cannot be further simplified but can be directly computed numerically if the mismatch ΔL is comparable with eV . In this instance, the shot noise and current profiles will be distorted, but the profile evolution will remain intact.

B. QD in the Coulomb blockade or Kondo regime

When taking into account the Coulomb interaction U between electrons in the QD, one may question if Fano resonances can be observed in transport spectra of a MZFI. We believe that the formalism is applicable to an interacting resonant level that can be described by a single level Anderson model and thus Fano resonances persist even if an interacting QD is involved. If not considering possible quantum phase transitions, chiral electrons always go through the point where the QD is side-coupled. This imposes a strict constraint on the formalism. In the case of a noninteracting QD, the bare propagator along the upper edge is $g_{uu}^r(x, x') = g_{uu}^{0r}(x, x')\tau_d(\epsilon)$, $\tau_d(\epsilon) = 1 - 2i\Gamma g_{dd}^r = \frac{\epsilon - \epsilon_d - i\Gamma}{\epsilon - \epsilon_d + i\Gamma}$ provided $g_{dd}^r(\epsilon) = [(g_{dd}^{0r}(\epsilon))^{-1} - \Sigma_d(\epsilon)]^{-1} = (\epsilon - \epsilon_d + i\Gamma)^{-1}$. The details are given in Appendix A 4. If the Coulomb interaction is present, one must resort to approximate schemes to tackle this problem. Modifying the Green's function of the isolated QD is a clumsy but sensible solution under the constraint $Im\Sigma_d(\epsilon) = -i\Gamma$. One can choose $Re\Sigma_d(\epsilon) = 0$ and $g_{dd}^{0r}(\epsilon) = (1 - n_d)(\epsilon - \epsilon_d + i0^+)^{-1} + n_d(\epsilon - \epsilon_d - U + i0^+)^{-1}$ in the Coulomb blockade regime[50, 51], $g_{dd}^{0r}(\epsilon) = (\epsilon - \epsilon_d + i0^+)^{-1}$ and $\epsilon - \epsilon_d - Re\Sigma_d(\epsilon) = (\epsilon - \alpha)\Gamma/(2k_B T_K)$ in the Kondo regime[9, 52]. Here, T_K is the Kondo temperature, α is a constant, and n_d is the occupation number of the resonant level ϵ_d . Thus, one may convince himself that even in the case when the QD is in the equilibrium the Coulomb blockade regime or Kondo regime, fully tunable Fano resonances could be expected.

V. CONCLUDING REMARKS

To summarize, our results indicate that Fano resonances in chiral electron transport require an extra direct path to emerge. Motivated by this finding, we suggest an electronic MZFI, which is possibly the simplest and cleanest setting to explore the Fano effect in chiral electronic transport. Despite their simplicity, fully tun-

able Fano resonances can be easily achieved by altering an external magnetic field in almost all transport spectra of this simple arrangement. They are robust with respect to device parameters such as interedge couplings, edge-QD coupling, and arm lengths of the interferometer. Therefore, parameters to fit Fano profiles of transport spectra are not needed in chiral electronic transport. Future directions would be of great interest in adapt it to a more intricate edge structure such as the edge modes in the fractional quantum hall systems and studying the Fano effect in transport through an asymmetric MZFI under decoherence. Another possibility could be developing more accurate analytical and numerical approaches to examine the overlapped Fano resonances with a multi-level QD and the Fano effect with a strongly correlated QD.

ACKNOWLEDGMENTS

This work is supported by National Natural Science Foundation of China (Grant No. 12464019) and Science and Technology Research Project of Jiangxi Provincial Department of Education (Grant No. GJJ2200324).

Appendix A: Derivation of the current Eq. (2) in the absence of contact Hamiltonian

In this Appendix, we present a detailed derivation of the current (2) without considering the contact Hamiltonian, based on the equation-of-motion method and the Keldysh technique. Sec. A 1 shows the details of how to obtain Dyson's equations for the various full retarded Green's functions from their equations of motion. The Keldysh equation for the lesser Green's function of the upper edge is given in Sec. A 2. Sec. A 3 gives the expressions for the various bare Green's functions of the isolated edges in the absence of a QD. Modified retarded Green's functions of the isolated upper edge with a side-attached QD are presented in Sec. A 4. In Sec. A 5 we calculate the various full retarded Green's functions and present their explicit expressions. Finally we derive Eq. (2) in Sec. A 6.

1. Dyson's equations for the full retarded Green's functions of the edges

In this section we give a detailed derivation of Dyson's equations for the full propagators (retarded Green's functions) $G_{\alpha\beta}^r(x, t; x', t')$ ($\alpha, \beta = u, l$) with the equation-of-motion method. The full propagators are defined as

$$G_{\alpha\beta}^r(x, t; x', t') = -\frac{i}{\hbar}\theta(t - t')\langle\{\hat{\psi}_\alpha(x, t), \hat{\psi}_\beta^\dagger(x', t')\}\rangle_{H_D}.$$

As an example, we first consider the equation of motion for the propagator $G_{uu}^r(x, t; x', t')$ of the upper edge

$$i\hbar\partial_t G_{uu}^r(x, t; x', t') = -i\hbar v_F \partial_x G_{uu}^r(x, t; x', t') + \sum_{i=1,2} t_i G_{lu}^r(x_i, t; x', t') \delta(x - x_i) + \delta(t - t') \delta(x - x'), \quad (\text{A1})$$

where

$$G_{lu}^r(x_i, t; x', t') = -\frac{i}{\hbar} \theta(t - t') \langle \{ \hat{\psi}_l(x_i, t), \hat{\psi}_u^\dagger(x', t') \} \rangle_{H_D},$$

are the mixed propagators associated with both the upper and lower edges.

The retarded Green's functions of the isolated upper or lower edge are denoted by

$$g_{\alpha\alpha}^{0r}(x, x'; t) = -\frac{i}{\hbar} \theta(t - t') \langle \{ \hat{\psi}_\alpha(x, t), \hat{\psi}_\alpha^\dagger(x', t') \} \rangle_{H_\alpha},$$

To keep things simple, we take a decoupling scheme. First we consider the equation of motion for the propagators of the upper edge which is decoupled from the **QD**. The bare Green's functions of the isolated upper edge is denoted by g_{uu}^0 , and the Green's functions of the upper edge coupled to the **QD** but decoupled from the lower edge is denoted by g_{uu} , which can be easily obtained from the equation of motion without considering interedge tunneling. We leave this task in Sec. A4.

The equation of motion for $g_{uu}^{0r}(x, x'; t)$ reads

$$i\hbar\partial_t g_{uu}^{0r}(x, t; x', t') = \delta(t - t') \delta(x - x') + \theta(t) \langle \{ [\hat{\psi}_u(x, t), H_\alpha(x, t)], \hat{\psi}_u^\dagger(x', t') \} \rangle_{H_\alpha},$$

which can be simplified as

$$i\hbar(\partial_t + v_F \partial_x) g_{uu}^{0r}(x, t; x', t') = \delta(t - t') \delta(x - x'). \quad (\text{A2})$$

With this equation, Eq. (A1) can be cast in the following form

$$G_{uu}^r(x, t; x', t') = g_{uu}^{0r}(x, t; x', t') + \int d\tau \sum_{i=1,2} g_{uu}^{0r}(x, t; x_i, \tau) t_i G_{lu}^r(x_i, \tau; x', t'), \quad (\text{A3})$$

which is Fourier transformed to

$$G_{uu}^r(x, x'; \epsilon) = g_{uu}^{0r}(x, x'; \epsilon) + \sum_{i=1,2} g_{uu}^{0r}(x, x_i, \epsilon) t_i G_{lu}^r(x_i, x'; \epsilon). \quad (\text{A4})$$

Following the same procedure, one gets the equation for the mixed Green's functions $G_{lu}^r(x, x'; \epsilon)$

$$G_{lu}^r(x, x'; \epsilon) = \sum_{j=1,2} g_{ll}^{0r}(x, x_j, \epsilon) t_j^* G_{uu}^r(x_j, x'; \epsilon). \quad (\text{A5})$$

Substitution of Eq. (A5) into Eq. (A4) yields a standard Dyson's equation

$$G_{uu}^r(x, x'; \epsilon) = g_{uu}^{0r}(x, x'; \epsilon) + \sum_{i,j=1,2} g_{uu}^{0r}(x, x_i, \epsilon) \Sigma_u^r(x_i, x_j; \epsilon) G_{uu}^r(x_j, x'; \epsilon). \quad (\text{A6})$$

Here we have defined the retarded self-energies $\Sigma_u^r(x_i, x_j; \epsilon) = t_i t_j^* g_{ll}^{0r}(x_i, x_j, \epsilon)$ due to interedge tunneling.

If we set $x = x_i, x' = x_j$, Eq. (A6) is specified as

$$G_{uu}^r(x_i, x_j; \epsilon) = g_{uu}^{0r}(x_i, x_j; \epsilon) + \sum_{m,n=1,2} g_{uu}^{0r}(x_i, x_m, \epsilon) \Sigma_u^r(x_m, x_n; \epsilon) G_{uu}^r(x_n, x_j; \epsilon). \quad (\text{A7})$$

Referring the terms associated with arguments x_i and $x_j, i, j = 1, 2$, to the elements of 2×2 matrices, we can rewrite the above equation in matrix form

$$\hat{G}_{uu}^r(\epsilon) = \hat{g}_{uu}^{0r}(\epsilon) + \hat{g}_{uu}^{0r}(\epsilon) \hat{\Sigma}_u^r(\epsilon) \hat{G}_{uu}^r(\epsilon).$$

From now on we suppress the argument ϵ for easy representation and recover it when necessary. Solving for $G_{uu}^r(x_i, x_j)$ in terms of \hat{g}_{uu}^{0r} gives

$$\begin{aligned} G_{uu}^r(x_i, x_j) &= \sum_k [(\hat{1} - \hat{g}_{uu}^{0r} \hat{\Sigma}_u^r)^{-1}]_{ik} g_{uu}^{0r}(x_k, x_j) \\ &= \sum_k g_{uu}^{0r}(x_i, x_k) [(\hat{1} - \hat{\Sigma}_u^r \hat{g}_{uu}^{0r})^{-1}]_{kj}. \end{aligned} \quad (\text{A8})$$

Setting $x = x_i$, we proceed by iteration

$$\begin{aligned} G_{uu}^r(x_i, x') &= g_{uu}^{0r}(x_i, x') + \sum_{jk} g_{uu}^{0r}(x_i, x_j) \Sigma_u^r(x_j, x_k) \\ &\quad g_{uu}^{0r}(x_k, x') + \sum_{jkmn} g_{uu}^{0r}(x_i, x_j) \Sigma_u^r(x_j, x_k) \\ &\quad g_{uu}^{0r}(x_k, x_m) \Sigma_u^r(x_m, x_n) g_{uu}^{0r}(x_n, x') \dots \end{aligned} \quad (\text{A9})$$

It is easy to convince oneself that the infinite order iteration results in

$$G_{uu}^r(x_i, x') = \sum_j [(\hat{1} - \hat{g}_{uu}^{0r} \hat{\Sigma}_u^r)^{-1}]_{ij} g_{uu}^{0r}(x_j, x'). \quad (\text{A10})$$

Analogously one has

$$G_{uu}^r(x, x_j) = \sum_i g_{uu}^{0r}(x, x_i) [(\hat{1} - \hat{\Sigma}_u^r \hat{g}_{uu}^{0r})^{-1}]_{ij}. \quad (\text{A11})$$

Substitution of Eq. (A10) into Eq. (A6) allows us to express the propagators of the upper edge in terms of the bare ones

$$G_{uu}^r(x, x'; \epsilon) = g_{uu}^{0r}(x, x'; \epsilon) + \sum_{i,j} g_{uu}^{0r}(x, x_i, \epsilon) \hat{\mathcal{Y}}_u^r(x_i, x_j, \epsilon) g_{uu}^{0r}(x_j, x'; \epsilon), \quad (\text{A12})$$

where we have introduced an improper retarded self-energy matrix $\hat{\mathcal{Y}}_u^r = \hat{\Sigma}_u^r (\hat{1} - \hat{g}_{uu}^{0r} \hat{\Sigma}_u^r)^{-1}$.

The propagators of the lower edge can be obtained in a similar manner

$$G_{ll}^r(x, x'; \epsilon) = g_{ll}^{0r}(x, x'; \epsilon) + \sum_{i,j} g_{ll}^{0r}(x, x_i, \epsilon) \mathcal{Z}_l^r(x_i, x_j; \epsilon) g_{ll}^r(x_j, x'; \epsilon), \quad (\text{A13})$$

where $\mathcal{Z}_l^r = \Sigma_l^r (\hat{1} - \hat{g}_{ll}^{0r} \hat{\Sigma}_l^r)^{-1}$ is the improper retarded self-energy associated with the retarded Green's functions of the lower edge, and $\Sigma_l^r(x_i, x_j; \epsilon) = t_i^* t_j g_{uu}^{0r}(x_i, x_j, \epsilon)$ are the corresponding retarded self-energies.

Inserting Eq. (A10) into Eq. (A5), we get the expression for the mixed propagators $G_{lu}^r(x, x'; \epsilon)$ from the upper edge to the lower edge

$$G_{lu}^r(x, x'; \epsilon) = \sum_{i,j=1,2} g_{ll}^{0r}(x, x_i, \epsilon) t_i^* [(\hat{1} - \hat{g}_{uu}^{0r} \hat{\Sigma}_u^r)^{-1}]_{ij} g_{uu}^{0r}(x_j, x', \epsilon). \quad (\text{A14})$$

The mixed propagators $G_{ul}^r(x, x'; \epsilon)$ from the lower edge to the upper edge are derived as

$$G_{ul}^r(x, x'; \epsilon) = \sum_{i,j=1,2} g_{uu}^{0r}(x, x_i, \epsilon) t_i [(\hat{1} - \hat{g}_{ll}^{0r} \hat{\Sigma}_l^r)^{-1}]_{ij} g_{ll}^{0r}(x_j, x', \epsilon). \quad (\text{A15})$$

2. The lesser Green's functions of the upper edge

The strategy to find a lesser Green's function $G^<$ is to apply the Langreth rules[51] to the integral equation for the retarded one. Infinite order iteration of the resultant integral equation will lead to the keldysh equation for the lesser Green's function. Starting with Eq. (A6) for the retarded Green's function $G_{uu}^r(x, x'; \epsilon)$, We formulate it in algebraic form

$$G^r = g^r + g^r \Sigma^r G^r, \quad (\text{A16})$$

where we suppressed the subscripts uu for simplicity and recover them when necessary. Applying the Langreth rule $(AB)^< = A^r B^< + A^< B^a$ to Eq. (A16), we obtain the equation for the lesser Green's function $G^<$

$$G^< = g^< + g^< \Sigma^a G^a + g^r \Sigma^< G^a + g^r \Sigma^r G^<. \quad (\text{A17})$$

This equation can be iterated, and the infinite order iteration results in the well-known Keldysh equation

$$G^< = (1 + G^r \Sigma^r) g^< (1 + \Sigma^a G^a) + G^r \Sigma^< G^a. \quad (\text{A18})$$

Using the relations $g^< = f(\epsilon)(g^a - g^r)$, $1 + G^r \Sigma^r = G^r (g^r)^{-1}$ and $1 + \Sigma^a G^a = (g^a)^{-1} G^a$, the keldysh equation (A18) is transformed into

$$G^< = f(\epsilon)(G^a - G^r) + \hat{G}^r f(\epsilon)(\Sigma^r - \Sigma^a) G^a + G^r \Sigma^< G^a. \quad (\text{A19})$$

For chiral electrons, the retarded (or advanced) Green's function propagating from x back to x is the same as its isolated counterpart, i.e., $G_{uu}^{r/a}(x, x; \epsilon) = g_{uu}^{0r/a}(x, x; \epsilon)$. As a consequence, the above Keldysh equation can be further simplified into

$$G_{uu}^<(x, x) = [f_{S_1}(\epsilon) - f_{eq}(\epsilon)] [g_{uu}^a(x, x) - g_{uu}^r(x, x)] + \sum_{i,j} G_{uu}^r(x, x_i) \Sigma_{u,ij}^< G_{uu}^a(x_j, x). \quad (\text{A20})$$

Here we have defined a lesser self-energy matrix $\hat{\Sigma}_u^<$

$$\Sigma_{u,ij}^< = \Sigma_u^<(x_i, x_j) = i[f_{S_2}(\epsilon) - f_{S_1}(\epsilon)] \Gamma^u(x_i, x_j), \quad (\text{A21})$$

with coupling matrix elements given by

$$\Gamma^u(x_i, x_j) = i[\Sigma_u^r(x_i, x_j) - \Sigma_u^a(x_i, x_j)]. \quad (\text{A22})$$

Notice that an equilibrium term $f_{eq}(g^a - g^r)$ in Eq. (A20) has been discarded, since it does not contribute to current.

3. Various bare Green's functions of the isolated edges

In order to find the various full Green's functions, one needs to know the bare ones of the isolated edges. We first derive these functions in the absence of a QD. The mode expansion of chiral field operators in the thermodynamical limit may be written as

$$\hat{\psi}_\alpha(x, t) = \int_{-\infty}^{+\infty} \frac{dk}{2\pi} \hat{c}_\alpha(k) e^{ik(x - v_F t)}, \quad \alpha = u, l \quad (\text{A23})$$

where $\hat{c}_\alpha(k)$ is the annihilation operator for a state with wave number k on the edge α . Then one arrives at

$$\begin{aligned} g_{\alpha\alpha}^{0r}(x, t; x', t') &= -\frac{i}{\hbar} \theta(t - t') \langle \{ \hat{\psi}_\alpha(x, t), \hat{\psi}_\alpha^\dagger(x', t') \} \rangle_0 \\ &= -\frac{i}{\hbar} \theta(t - t') \int_{-\infty}^{+\infty} \frac{dk}{2\pi} e^{-iv_F k(t-t')} e^{ik(x-x')}, \end{aligned}$$

Fourier transform of which gives

$$g_{\alpha\alpha}^{0r}(x, x'; \epsilon) = -\frac{i}{\hbar v_F} \theta(x - x') e^{i\epsilon(x-x')/\hbar v_F}. \quad (\text{A24})$$

The corresponding advanced and lesser Green's functions can be calculated by direct substitution

$$g_{\alpha\alpha}^{0a}(x, x'; \epsilon) = \frac{i}{\hbar v_F} \theta(x' - x) e^{i\epsilon(x-x')/\hbar v_F}, \quad (\text{A25})$$

$$g_{\alpha\alpha}^{0<}(x, x'; \epsilon) = \frac{i}{\hbar v_F} f_{S_\alpha}(\epsilon) e^{i\epsilon(x-x')/\hbar v_F}, \quad (\text{A26})$$

where $f_{S_\alpha}(\epsilon) = f(\epsilon - \mu_{S_\alpha})$ is the Fermi-Dirac distribution function of the source S_α , which injects electrons in the edge, $\alpha = u, l$. In our setup, $S_u = S_1, S_l = S_2$ and

$D_u = D_1, D_l = D_2$. For this reason, $\alpha = u, l$ and $i = 1, 2$ are adopted interchangeably to label the contacts.

Since

$$g_{\alpha\alpha}^{0a}(x, x'; \epsilon) - g_{\alpha\alpha}^{0r}(x, x'; \epsilon) = \frac{i}{\hbar v_F} e^{i\epsilon(x-x')/\hbar v_F}, \quad (\text{A27})$$

the lesser Green's functions can be rewritten in a desired form

$$g_{\alpha\alpha}^{0<}(x, x'; \epsilon) = f_{S_\alpha} [g_{\alpha\alpha}^{0a}(x, x'; \epsilon) - g_{\alpha\alpha}^{0r}(x, x'; \epsilon)]. \quad (\text{A28})$$

To apply Eq. (A28) to non-equilibrium transport problems, it will be proved to be useful to make the following decomposition since the current depends only on the difference of distribution functions

$$g_{\alpha\alpha}^{0<}(x, x'; \epsilon) = f_{eq} [g_{\alpha\alpha}^{0a}(x, x'; \epsilon) - g_{\alpha\alpha}^{0r}(x, x'; \epsilon)] + [f_{S_\alpha} - f_{eq}] [g_{\alpha\alpha}^{0a}(x, x'; \epsilon) - g_{\alpha\alpha}^{0r}(x, x'; \epsilon)], \quad (\text{A29})$$

where $f_{eq}(\epsilon)$ is the distribution function in equilibrium and thus the first term makes no contribution to current.

4. The retarded Green's functions of the upper edge with a side-attached quantum dot

If a QD with a localized level ϵ_d is side-attached to the upper edge, the Hamiltonian for the isolated upper edge H_u is replaced by $H_u + H_d + H_{ud}$. The retarded Green's functions of the isolated upper edge are denoted by g^{0r} and those coupled to a QD by g^r . They are related by ($x' < x_d < x$)

$$g_{uu}^r(x, x'; \epsilon) = g_{uu}^{0r}(x, x'; \epsilon) + g_{uu}^{0r}(x, x_d; \epsilon) t_d g_{du}^r(x_d, x'; \epsilon). \quad (\text{A30})$$

The mix Green's functions associated with the dot and the upper edge $g_{du}^r(x_d, x'; \epsilon)$ satisfy

$$g_{du}^r(x_d, x'; \epsilon) = g_{dd}^r(\epsilon) t_d g_{uu}^{0r}(x_d, x'; \epsilon). \quad (\text{A31})$$

We also have equations for the retarded Green's function of the QD $g_{dd}^r(\epsilon)$ and the mixed Green's function $g_{ud}^r(x_d, x_d; \epsilon)$

$$g_{dd}^r(\epsilon) = g_{dd}^{0r}(\epsilon) [1 + t_d g_{ud}^r(x_d, x_d; \epsilon)], \quad (\text{A32})$$

$$g_{ud}^r(x_d, x_d; \epsilon) = g_{uu}^{0r}(x_d, x_d; \epsilon) t_d g_{dd}^r(\epsilon), \quad (\text{A33})$$

where g_{dd}^{0r} is the retarded Green's function of the isolated QD. Now we solve for $g_{dd}^r(\epsilon)$ by substituting Eq. (A33) into (A32) and find

$$g_{dd}^r(\epsilon) = \frac{1}{[g_{dd}^{0r}(\epsilon)]^{-1} - \Sigma_d^r(\epsilon)}. \quad (\text{A34})$$

The retarded Green's function of the isolated QD is $g_{dd}^{0r}(\epsilon) = (\epsilon - \epsilon_d + i0^+)^{-1}$, and the self-energy of the retarded Green's function of the QD due to edge-dot coupling is given by

$$\Sigma_d^r(\epsilon) = t_d^2 g_{uu}^{0r}(x_d, x_d; \epsilon) = -i \frac{t_d^2}{2\hbar v_F} = -i \frac{\hbar v_F \gamma_d^2}{d} = -i\Gamma. \quad (\text{A35})$$

Note that we have assumed $\theta(0) = 1/2$ and thereby $g_{\alpha\alpha}^r(x, x; \epsilon) = \frac{1}{i2\hbar v_F}$. The retarded Green's function on the dot takes a simple expression

$$g_{dd}^r(\epsilon) = \frac{1}{\epsilon - \epsilon_d + i\Gamma}. \quad (\text{A36})$$

Plugging Eqs. (A24), (A31) and (A36) into Eq. (A30), we get an explicit expression for the retarded Green's functions of the isolated upper edge in the presence of a side-coupled QD for $x' < x_d < x$

$$g_{uu}^r(x, x', \epsilon) = -\frac{i}{\hbar v_F} e^{i\epsilon(x-x')/\hbar v_F} \theta(x-x') \frac{\epsilon - \epsilon_d - i\Gamma}{\epsilon - \epsilon_d + i\Gamma}. \quad (\text{A37})$$

The assumption $\theta(0) = 1/2$ used to obtain the expression for the self-energy Eq. (A35) of the dot's Green's function is not trivial but even subtle. If we view $\frac{\epsilon - \epsilon_d - i\Gamma}{\epsilon - \epsilon_d + i\Gamma}$ as the transmission amplitude $\tau_d(\epsilon)$ across the point x_d , the transmission probability must be always one, irrespective of the electron's incident energy, because there is no mechanism for the electron to reflect back. Otherwise we will find a less-than-one transmission probability with an amplitude $\tau_d(\epsilon) = \frac{\epsilon - \epsilon_d}{\epsilon - \epsilon_d + i\Gamma}$ if assuming $\theta(0) = 1$. It contradicts the fact that chiral electrons always go through the point to which the QD is side-attached. In Appendix C, we will confirm this result using the scattering matrix approach.

The effect resulting from the presence of a side-attached QD is incorporated into the Green's functions of the isolated upper edge as a transmission amplitude of unit modulus with an incident-energy-dependent phase, since the straight-through transmission probability across x_d is obviously unity. Eq. (A37) may be repressed in the manner

$$g_{uu}^r(x, x', \epsilon) = -\frac{i}{\hbar v_F} e^{i\epsilon(x-x')/\hbar v_F} \theta(x-x') \tau_d(\epsilon), \quad (\text{A38})$$

for $x' < x_d < x$, and $g_{uu}^r(x, x', \epsilon) = g_{uu}^{r0}(x, x', \epsilon)$ for other configurations,

5. Explicit expressions for the full propagators

We present explicit expressions for the various retarded Green's functions in this section, which will be useful in the subsequent applications. For convenience, we denote the matrix functions appearing in Eqs. (A10), (A11), (A15) by $\hat{A}, \hat{B}, \hat{C}$, respectively: $\hat{A} = (\hat{1} - \hat{\Sigma}_u^r \hat{g}_{uu}^r)^{-1}$, $\hat{B} = (\hat{1} - \hat{g}_{uu}^r \hat{\Sigma}_u^r)^{-1}$, $\hat{C} = (\hat{1} - \hat{g}_{ll}^r \hat{\Sigma}_l^r)^{-1}$. They are derived readily as

$$\hat{X} = \begin{bmatrix} \frac{1}{1+\gamma_1^2} & 0 \\ X_{21}(\epsilon) & \frac{1}{1+\gamma_2^2} \end{bmatrix}, X = A, B, C \quad (\text{A39})$$

with non-diagonal elements given by

$$\begin{aligned} A_{21}(\epsilon) &= \frac{-2[\gamma_2^2 \tau_d(\epsilon) e^{i\epsilon L_u/\hbar v_F} + \gamma_1 \gamma_2 e^{i(2\pi \frac{\Phi}{\Phi_0} + \epsilon L_l/\hbar v_F)}]}{(1 + \gamma_1^2)(1 + \gamma_2^2)}, \\ B_{21}(\epsilon) &= \frac{-2[\gamma_1^2 \tau_d(\epsilon) e^{i\epsilon L_u/\hbar v_F} + \gamma_1 \gamma_2 e^{i(2\pi \frac{\Phi}{\Phi_0} + \epsilon L_l/\hbar v_F)}]}{(1 + \gamma_1^2)(1 + \gamma_2^2)}, \\ C_{21}(\epsilon) &= \frac{-2[\gamma_1^2 e^{i\epsilon L_l/\hbar v_F} + \gamma_1 \gamma_2 \tau_d(\epsilon) e^{-i(2\pi \frac{\Phi}{\Phi_0} - \epsilon L_u/\hbar v_F)}]}{(1 + \gamma_1^2)(1 + \gamma_2^2)}, \end{aligned}$$

where Φ is the magnetic flux enclosed by two arms of the **MZFI** and $\Phi_0 = hc/e$ is the flux quantum.

Substituting Eqs. (A24), (A39) into Eq. (A11), we obtain the following two propagators $G_{uu}^r(x, x_i; \epsilon)$ ($x_1 <$

$x_2 < x$)

$$G_{uu}^r(x, x_2; \epsilon) = -\frac{i}{\hbar v_F(1 + \gamma_2^2)} e^{i\epsilon(x-x_2)/\hbar v_F}, \quad (\text{A40})$$

and

$$\begin{aligned} G_{uu}^r(x, x_1; \epsilon) &= -\frac{i\tau_d(\epsilon)}{\hbar v_F(1 + \gamma_1^2)} e^{i\epsilon(x-x_1)/\hbar v_F} \\ &\quad - A_{21}(\epsilon) \frac{i}{\hbar v_F} e^{i\epsilon(x-x_2)/\hbar v_F}. \end{aligned} \quad (\text{A41})$$

It is these two retarded Green's functions that will be used to evaluate the current flowing into drain D_1 in Sec. A6.

Another four useful propagators are $G_{\alpha\beta}^r(x, x'; \epsilon)$ ($x' < x_1 < x_2 < x$), and are obtained after back substitution of Eqs. (A24) and (A39) into (A12)-(A15), respectively

$$G_{uu}^r(x, x'; \epsilon) = \frac{e^{i\epsilon(x-x')/\hbar v_F}}{i\hbar v_F} [\sqrt{R_1 R_2} \tau_d(\epsilon) - \sqrt{T_1 T_2} e^{i(2\pi \frac{\Phi}{\Phi_0} + \epsilon \Delta L/\hbar v_F)}], \quad (\text{A42})$$

$$G_{ll}^r(x, x'; \epsilon) = \frac{e^{i\epsilon(x-x')/\hbar v_F}}{i\hbar v_F} [\sqrt{R_1 R_2} - \sqrt{T_1 T_2} \tau_d(\epsilon) e^{-i(2\pi \frac{\Phi}{\Phi_0} + \epsilon \Delta L/\hbar v_F)}], \quad (\text{A43})$$

$$G_{lu}^r(x, x'; \epsilon) = -\frac{e^{i\epsilon(x-x')/\hbar v_F}}{\hbar v_F} [\sqrt{R_1 T_2} \tau_d(\epsilon) + \sqrt{T_1 R_2} e^{i(2\pi \frac{\Phi}{\Phi_0} + \epsilon \Delta L/\hbar v_F)}], \quad (\text{A44})$$

$$G_{ul}^r(x, x'; \epsilon) = -\frac{e^{i\epsilon(x-x')/\hbar v_F}}{\hbar v_F} [\sqrt{R_1 T_2} + \sqrt{T_1 R_2} \tau_d(\epsilon) e^{-i(2\pi \frac{\Phi}{\Phi_0} + \epsilon \Delta L/\hbar v_F)}], \quad (\text{A45})$$

where $\delta L = L_l - L_u$ is the length difference of the lower and upper arms of the **MZFI**, $T_i = 4\gamma_i^2/(1 + \gamma_i^2)^2$ and $R_i = (1 - \gamma_i^2)^2/(1 + \gamma_i^2)^2$ are the transmission and reflection coefficients of carriers at **QPCi**.

6. Current flowing into drain D_1

In this section, we derive an explicit expression for the current I_{D_1} flowing into D_1 . One may choose the Fermi-Dirac distribution function $f_{D_1} = f(\epsilon - \mu_{D_1}) = 1/[e^{(\epsilon - \mu_{D_1})/k_B T} + 1]$ of D_1 as the equilibrium distribution function $f_{eq}(\epsilon)$, and obtains after inserting the lesser Green's function (A20) of the upper edge into current expression (1)

$$\begin{aligned} I_{D_1} &= I_{D_1}^0 + \frac{e}{h} \int_{-\infty}^{+\infty} d\epsilon [f_{S_2}(\epsilon) - f_{S_1}(\epsilon)] i\hbar v_F \\ &\quad \sum_{i,j} G_{uu}^r(x, x_i; \epsilon) \Gamma_{ij}^u(\epsilon) G_{uu}^a(x_j, x; \epsilon), \end{aligned} \quad (\text{A46})$$

where

$$I_{D_1}^0 = \frac{e}{h} \int_{-\infty}^{+\infty} d\epsilon [f_{D_1}(\epsilon) - f_{S_1}(\epsilon)], \quad (\text{A47})$$

is the direct current contributed by chiral electrons injected from the source S_1 without tunneling into the lower edge or the **QD**.

It is suggestive to rewrite the above equation into the Landauer-Büttiker form

$$\begin{aligned} I_{D_1} &= \frac{e}{h} \int_{-\infty}^{+\infty} d\epsilon \{ [f_{D_1}(\epsilon) - f_{S_1}(\epsilon)] \mathcal{T}_{D_1 S_1}(\epsilon) + \\ &\quad [f_{D_1}(\epsilon) - f_{S_2}(\epsilon)] \mathcal{T}_{D_1 S_2}(\epsilon) \}. \end{aligned} \quad (\text{A48})$$

In Eq. (A48), $\mathcal{T}_{D_j S_i}(\epsilon)$, $i, j = 1, 2$ are the transmission probabilities for chiral electrons tunneling through the device from lead S_i to lead D_j , and given by

$$\begin{aligned} \mathcal{T}_{D_1 S_i}(\epsilon) &= \delta_{1i} + (-1)^{\delta_{1i}} \hbar v_F \sum_{m,n} G_{uu}^r(x, x_m; \epsilon) \Gamma_{mn}^u(\epsilon) \\ &\quad G_{uu}^a(x_n, x; \epsilon), \quad i = 1, 2. \end{aligned} \quad (\text{A49})$$

where the coupling matrix elements are found to be

$$\Gamma_{ij}^u(\epsilon) = 4\hbar v_F \gamma_i \gamma_j e^{-i(2\pi \frac{\Phi}{\Phi_0} + \epsilon L_l/\hbar v_F)(1 - \delta_{ij})}. \quad (\text{A50})$$

There are two contributions to the current flowing into D_1 , obviously from in Eq. (A48): source S_1 and source S_2 . From their definitions, we may infer that $G^r(x_i, x_j) = [G^a(x_j, x_i)]^*$ and $\Gamma_u(x_i, x_j) = [\Gamma_u(x_j, x_i)]^*$. We calculate each term in Eq. (A49) and obtain

$$\begin{aligned}
\hbar v_F \Gamma_{22}^u(\epsilon) |G_{uu}^r(x, x_2; \epsilon)|^2 &= \frac{4\gamma_2^2}{(1 + \gamma_2^2)^2}, \\
\hbar v_F \Gamma_{11}^u(\epsilon) |G_{uu}^r(x, x_1; \epsilon)|^2 &= \frac{4\gamma_1^2}{(1 + \gamma_1^2)^2 (1 + \gamma_2^2)^2} \left[(1 - \gamma_2^2)^2 |\tau_d(\epsilon)|^2 + 4\gamma_1^2 \gamma_2^2 - 4\gamma_1 \gamma_2 (1 - \gamma_2^2) \right. \\
&\quad \left. \text{Re} [\tau_d(\epsilon) e^{-i(2\pi \frac{\Phi}{\Phi_0} + \epsilon \Delta L / \hbar v_F)}] \right], \\
\hbar v_F \text{Re} [\Gamma_{12}^u(G_{uu}^r(x, x_1; \epsilon) G_{uu}^a(x_2, x; \epsilon))] &= \frac{4\gamma_1 \gamma_2}{(1 + \gamma_1^2)(1 + \gamma_2^2)^2} \left[-2\gamma_1 \gamma_2 + (1 - \gamma_2^2) \text{Re} [\tau_d(\epsilon) e^{-i(2\pi \frac{\Phi}{\Phi_0} + \epsilon \Delta L / \hbar v_F)}] \right].
\end{aligned}$$

Substituting the above three terms back into Eq. (A49) and regrouping similar terms, the transmission probability is found to be the squared magnitude of a transmission amplitude

$$\begin{aligned}
\mathcal{T}_{D_1 S_2}(\epsilon) &= |\sqrt{R_1 T_2} + \sqrt{T_1 R_2} \tau_d(\epsilon) e^{-i(\phi_{AB} + \epsilon \Delta L / \hbar v_F)}|^2, \\
\mathcal{T}_{D_1 S_1}(\epsilon) &= 1 - \mathcal{T}_{D_1 S_2}(\epsilon). \tag{A51}
\end{aligned}$$

Appendix B: Current expression in the presence of contact Hamiltonian

In this section, we consider a standard set up: a central scattering region (the device) is connected via leads to contacts as reservoirs. The Hamiltonian can be decomposed as $H = H_C + H_D + H_T$, where H_D is the device Hamiltonian given in the main text, H_C represents the Hamiltonian of the contacts, and H_T is the coupling Hamiltonian between the device and the leads. The leads are modeled by one-dimensional chiral edge states and described by the chiral Hamiltonian

$$H_C = -i \sum_{\alpha=u,l}^{i=S,D} \hbar v_F^{i_\alpha} \int dy \hat{\varphi}_{i_\alpha}^\dagger(y) \partial_x \hat{\varphi}_{i_\alpha}(y), \tag{B1}$$

where $\hat{\varphi}_{i_\alpha}(y)$ are the field operators for lead i_α . The chemical potential of contact i_α is μ_{i_α} , where $i = S, D$ and $\alpha = u, l$ (or 1, 2). The couplings between the leads and the device are given by the tunneling Hamiltonian

$$H_T = \sum_{\alpha=u,l}^{i=S,D} [t_{i_\alpha} \hat{\varphi}_{i_\alpha}^\dagger(y_L) \hat{\psi}_\alpha(x_L) + H.c.], \tag{B2}$$

where x_L, x_R and y_L, y_R are, respectively, the positions at which the central device and the leads are connected.

The current flowing into the upper drain D_1 can be calculated from the time evolution of the number operator of the upper drain D_1 :

$$\begin{aligned}
I_{D_1} &= e \frac{d}{dt} \int dy \langle \hat{\varphi}_{D_u}^\dagger(y, t) \hat{\varphi}_{D_u}(y, t) \rangle_H \\
&= -\frac{ie}{\hbar} [t_{D_u} \langle \hat{\varphi}_{D_u}^\dagger(y_R, t) \hat{\psi}_u(x_R, t) \rangle_H - H.c.] \tag{B3}
\end{aligned}$$

With the definition of the lesser Green's function $\mathcal{G}_{uD}^<(x, t'; y, t) = \frac{i}{\hbar} \langle \hat{\varphi}_{D_u}^\dagger(y, t) \hat{\psi}_u(x, t') \rangle_H$, the above equation can be rewritten as

$$I_{D_1} = -2e \text{Re} [t_{D_u} \mathcal{G}_{uD}^<(x_R, t; y_R, t)]. \tag{B4}$$

The equation of motion for the mixed retarded Green's function $\mathcal{G}_{uD}^r(x_R, y_R; \epsilon)$ gives

$$\mathcal{G}_{uD}^r(x_R, y_R; \epsilon) = \mathcal{G}_{uu}^r(x_R, x_R; \epsilon) t_{D_u}^* \mathcal{G}_{D_u}^r(y_R, y_R; \epsilon). \tag{B5}$$

The corresponding lesser Green's function is found by applying the Langreth rules

$$\begin{aligned}
\mathcal{G}_{uD}^<(x_R, y_R; \epsilon) &= \mathcal{G}_{uu}^r(x_R, x_R; \epsilon) t_{D_u}^* \mathcal{G}_{D_u}^<(y_R, y_R; \epsilon) + \\
&\quad \mathcal{G}_{uu}^<(x_R, x_R; \epsilon) t_{D_u}^* \mathcal{G}_{D_u}^r(y_R, y_R; \epsilon) \tag{B6}
\end{aligned}$$

Eq. (B3) becomes after inserting Eq. (B6) into Eq. (B3)

$$\begin{aligned}
I_{D_1} &= -2e \int \frac{d\epsilon}{2\pi\hbar} \text{Re} [\mathcal{G}_{uu}^r(x_R, x_R; \epsilon) \Xi_u^<(y_R, y_R; \epsilon) + \\
&\quad \mathcal{G}_{uu}^<(x_R, x_R; \epsilon) \Xi_u^a(y_R, y_R; \epsilon)], \tag{B7}
\end{aligned}$$

where $\Xi_u^{r,a,<}(x_m, x_m; \epsilon) = |t_{mu}|^2 g_{mu}^{r,a,<}(y_m, y_m; \epsilon)$, $m = L, R$ are various self-energies arising from the lead-upper-edge couplings. With the relation $G^r - G^a = G^> - G^<$, the above equation may be recast in another form

$$\begin{aligned}
I_{D_1} &= \frac{e}{\hbar} \int d\epsilon [\Xi_u^<(y_R, y_R; \epsilon) \mathcal{G}_{uu}^>(x_R, x_R; \epsilon) - \\
&\quad \Xi_u^>(y_R, y_R; \epsilon) \mathcal{G}_{uu}^<(x_R, x_R; \epsilon)]. \tag{B8}
\end{aligned}$$

In the presence of contacts, the Dyson's equation for the retarded Green's function $\mathcal{G}_{uu}^r(x, x'; \epsilon)$ is

$$\begin{aligned}
\mathcal{G}_{uu}^r(x, x'; \epsilon) &= \mathcal{G}_{uu}^{0r}(x, x'; \epsilon) + \sum_{m=L,R} \mathcal{G}_{uu}^{0r}(x, x_m, \epsilon) \\
&\quad \Xi_u^r(x_m, x_m; \epsilon) \mathcal{G}_{uu}^r(x_m, x'; \epsilon), \tag{B9}
\end{aligned}$$

where \mathcal{G}_{uu}^0 denotes the Green's function of the upper-edge in the absence of the lead-upper-edge couplings. From this equation one can obtain the following Keldysh equation

$$\begin{aligned} \mathcal{G}_{uu}^{</>}(x, x') &= \sum_{m,n=L,R} [\delta_{x,x_m} + \mathcal{G}_{uu}^r(x, x_m)\Xi_u^r(x_m, x_m)] \mathcal{G}_{uu}^{0</>}(x_m, x_n) [\delta_{x,x_n} + \Xi_u^a(x_n, x_n)\mathcal{G}_{uu}^a(x_n, x)] \\ &+ \sum_{m=L,R} \mathcal{G}_{uu}^r(x, x_m)\Xi_u^{</>}(x_m, x_m)\mathcal{G}_{uu}^a(x_m, x). \end{aligned} \quad (\text{B10})$$

The Green's function \mathcal{G}_{uu}^0 reduces to the Green's function G_{uu} if the lower edge is decoupled from the source $S_l(S_2)$ and the drain $D_l(D_2)$. One may get the Green's function \mathcal{G}_{uu}^0 from G_{uu} after replacing the decoupled Green's functions g_{ll}^0 from the lower contacts S_l, D_l by the coupled Green's functions g_{ll} to the lower contacts. Equation of motion for g_{ll}^r yields

$$\begin{aligned} g_{ll}^r(x, x'; \epsilon) &= g_{ll}^{0r}(x, x'; \epsilon) + \sum_{m=L,R} g_{ll}^{0r}(x, x_m; \epsilon)\Xi_l^r(y_m, y_m) \\ &g_{ll}^r(x_m, x'; \epsilon), \end{aligned} \quad (\text{B11})$$

where $\Xi_l^r(x_m, x_m; \epsilon) = |t_{ml}|^2 g_{ml}^r(y_m, y_m; \epsilon)$, $m = L, R$ are the retarded self-energies due to the lead-lower-edge couplings. It follows from Eq. (B11) that $g_{ll}^r(x_i, x_j; \epsilon) = g_{ll}^{0r}(x_i, x_j; \epsilon)$, $i, j = 1, 2$, $x_L < x_1, x_2 < x_R$, and $\mathcal{G}_{uu}^0(x, x') = G_{uu}^r(x, x')$. It justifies that the formalism in Appendix A to solve for full propagators through the device is reasonable from the propagators of the isolated upper and lower edges from contacts, even if we made an assumption that the edges are connected to the contacts. The corresponding Keldysh equation to Eq. (B11) reads

$$g_{ll}^<(x, x') = \sum_{m=L,R} g_{ll}^r(x, x_m)\Xi_l^<(y_m, y_m)g_{ll}^a(x_m, x'), \quad (\text{B12})$$

where $\Xi_l^{r,a,<}(x_m, x_m; \epsilon) = |t_{ml}|^2 g_{ml}^{r,a,<}(y_m, y_m; \epsilon)$, $m = L, R$. In addition, we have

$$\mathcal{G}_{uu}^{0<}(x, x') = \sum_{i,j} \mathcal{G}_{uu}^{0r}(x, x_i)\Sigma_{u,ij}^<(\epsilon)G_{uu}^{0a}(x_j, x'), \quad (\text{B13})$$

where $\Sigma_{u,ij}^<(\epsilon) = t_i t_j^* g_{ll}^<(x_i, x_j; \epsilon)$ is the lesser self-energy arising from the tunneling from the upper edge to the lower edge which is coupled to the contacts. Substituting

$$I_{D_1} = \frac{e}{h}(4\hbar v_F)^2 \int d\epsilon \{ [f_{D_1}(\epsilon) - f_{S_1}(\epsilon)](\gamma_{S_1}\gamma_{D_1})^2 |\mathcal{G}_{uu}^r(x_R, x_L)|^2 + [f_{D_1}(\epsilon) - f_{S_2}(\epsilon)](\gamma_{S_2}\gamma_{D_1})^2 |\mathcal{G}_{ul}^r(x_R, x_L)|^2 \}. \quad (\text{B18})$$

To obtain Eq. (B18) we have used the fact that $\mathcal{G}_{ul}^{r,a}(x_m, x_m) = 0$, $m = L, R$ for chiral electrons. Following the same procedure as we did in Appendix A 1, it is useful to rewrite the Dyson's equation Eq. (B9) for the retarded Green's functions $\mathcal{G}_{uu}^r(x_m, x_n)$, $m, n = L, R$ in matrix form $\hat{\mathcal{G}}_{uu}^r = \hat{\mathcal{G}}_{uu}^{0r} + \hat{\mathcal{G}}_{uu}^{0r}\hat{\Xi}_u^r\hat{\mathcal{G}}_{uu}^r$ with a diago-

Eq. (B12) and (B13) into Eq. (B10), Eq. (B10) becomes

$$\begin{aligned} \mathcal{G}_{uu}^{</>}(x, x') &= \sum_{m,n} \mathcal{G}_{ul}^r(x, x_m)\Xi_l^{</>}(x_m, x_m)\mathcal{G}_{lu}^a(x_m, x') + \\ &\sum_{m=L,R} \mathcal{G}_{uu}^r(x, x_m)\Xi_u^{</>}(x_m, x_m)\mathcal{G}_{uu}^a(x_m, x). \end{aligned} \quad (\text{B14})$$

Here we have used the relations:

$$\begin{aligned} \mathcal{G}_{ul}^r(x, x') &= \sum_i \mathcal{G}_{uu}^r(x, x_i)t_i g_{ll}^r(x_i, x'), \\ \mathcal{G}_{lu}^a(x, x') &= \sum_j g_{ll}^a(x, x_j)t_j^* \mathcal{G}_{uu}^a(x_j, x'). \end{aligned} \quad (\text{B15})$$

Similar to Eqs. (A24), (A26) and (A29) in Appendix A 3, the various Green's functions of the lead $m\alpha$ ($m = L, R$ or S, D ; $\alpha = u, l$ or $1, 2$) are given by

$$\begin{aligned} g_{m\alpha}^{a/r}(y_m, y_m; \epsilon) &= \frac{\pm i}{2\hbar v_F^{m\alpha}}, \\ g_{m\alpha}^<(y_m, y_m; \epsilon) &= \frac{i}{\hbar v_F^{m\alpha}} f_{m\alpha}(\epsilon), \\ g_{m\alpha}^>(y_m, y_m; \epsilon) &= \frac{i}{\hbar v_F^{m\alpha}} [1 - f_{m\alpha}(\epsilon)]. \end{aligned} \quad (\text{B16})$$

If we set the edge-lead coupling constant as $t_{m\alpha} = 2\hbar\sqrt{v_F v_F^{m\alpha}}\gamma_{m\alpha}$, $m = L, R$, $\alpha = u, l$, then the various self-energies due to edge-lead couplings are

$$\begin{aligned} \Xi_{\alpha}^{a/r}(y_m, y_m) &= \pm i 2\hbar v_F \gamma_{m\alpha}^2, \\ \Xi_{\alpha}^<(y_m, y_m) &= i 4\hbar v_F \gamma_{m\alpha}^2 f_{m\alpha}(\epsilon), \\ \Xi_{\alpha}^>(y_m, y_m) &= i 4\hbar v_F \gamma_{m\alpha}^2 [1 - f_{m\alpha}(\epsilon)]. \end{aligned} \quad (\text{B17})$$

Substituting Eq. (B14) and (B17) into Eq. (B8), we find

nal self-energy matrix $\hat{\Xi}_u^r = \text{dia}[\hat{\Xi}_u^r(x_L, x_L), \hat{\Xi}_u^r(x_R, x_R)]$.

Solving this matrix equation gives

$$\begin{aligned} \mathcal{G}_{uu}^r(x_R, x_L) &= \frac{1}{(1 + \gamma_{S_1}^2)(1 + \gamma_{D_1}^2)} \mathcal{G}_{uu}^{0r}(x_R, x_L) \\ &= \frac{1}{(1 + \gamma_{S_1}^2)(1 + \gamma_{D_1}^2)} G_{uu}^r(x_R, x_L). \end{aligned} \quad (\text{B19})$$

$$\mathcal{G}_{ul}^r(x_R, x_L) = \sum_{m,n=L,R} [(\hat{1} - \hat{\mathcal{G}}_{uu}^{0r} \hat{\Xi}_u^r)^{-1}]_{Rm} G_{ul}^r(x_m, x_n) [(\hat{1} - \hat{\Xi}_l^r \hat{g}_{ll}^{0r})^{-1}]_{nL} = \frac{1}{(1 + \gamma_{S_2}^2)(1 + \gamma_{D_1}^2)} G_{ul}^r(x_R, x_L). \quad (\text{B22})$$

With Eqs. (B20) and (B22) in hand, the current in Eq. (B18) reduces to

$$\begin{aligned} I_{D_1} &= \frac{e}{h} \int d\epsilon \left\{ [f_{D_1}(\epsilon) - f_{S_1}(\epsilon)] T_{S_1} \mathcal{T}_{D_1 S_1}(\epsilon) T_{D_1} \right. \\ &\quad \left. + [f_{D_1}(\epsilon) - f_{S_2}(\epsilon)] T_{S_2} \mathcal{T}_{D_1 S_2}(\epsilon) T_{D_1} \right\}, \end{aligned} \quad (\text{B23})$$

where $T_{m\alpha} = 4\gamma_{m\alpha}^2 / (1 + \gamma_{m\alpha}^2)^2$ is the transmission coefficient through the lead-edge contact $m\alpha$, and $\mathcal{T}_{D_1 S_i}(\epsilon) = |s_{D_1 S_i}|^2 = |i\hbar v_F G_{D_1 S_i}^r|^2 = |i\hbar v_F G_{u\alpha}^r(x_R, x_L)|^2$, $i = 1, 2$, $\alpha = u, l$ is the transmission coefficient from the top or bottom left to the top right of the device and can be easily understood from the Fisher-Lee relation.

If the edges are connected to the leads ballistically, i.e., the outer segments of edges are considered as leads, $\gamma_{m\alpha} = 1$, and thus $T_{S_i} = T_{D_1} = 1$, the current expression Eq. (B23) is the same as Eq. (A48) in Appendix A 6.

From Eq. (B23), one sees that each distribution function can be decomposed into $f_{m\alpha} = [f_{m\alpha} - f_{eq}] + f_{eq}$, and f_{eq} does not contribute to the current, since the current depends only on the difference of distribution functions. In addition, due to chiral nature of electron motion, the current flowing into a drain contact does not depend on the other drain contact. Therefore it is reasonable to omit the contribution from the drains when considering the lesser Green's functions of the edges, as we did in Appendix A.

Appendix C: Transmission amplitudes through x_d : A scattering matrix approach

In this section, we derive the transmission amplitude for chiral electrons passing through x_d on the upper edge

Also we have

$$\begin{aligned} \mathcal{G}_{uu}^r(x_R, x') &= \sum_{n=L,R} [(\hat{1} - \hat{\mathcal{G}}_{uu}^{0r} \hat{\Xi}_u^r)^{-1}]_{Rn} \mathcal{G}_{uu}^{0r}(x_n, x') \\ &= \sum_{n=L,R} [(\hat{1} - \hat{\mathcal{G}}_{uu}^{0r} \hat{\Xi}_u^r)^{-1}]_{Rn} G_{uu}^r(x_n, x'). \end{aligned} \quad (\text{B20})$$

To solve for $\mathcal{G}_{ul}^r(x, x_L)$, we also need to know $g_{ll}^r(x, x_L)$, which is found from Eq. (B11) to be

$$g_{ll}^r(x, x_L) = \sum_{n=L,R} g_{ll}^{0r}(x, x_n) [(\hat{1} - \hat{\Xi}_l^r \hat{g}_{ll}^{0r})^{-1}]_{nL}. \quad (\text{B21})$$

We finally obtain after plugging Eqs. (B20) and (B21) into Eq. (B15)

based on the scattering matrix approach and justify the assumption $\theta(0) = 1/2$ in Appendix A 3.

If the QD is absent, the transmission amplitude is obviously one. When the QD is side-attached to the upper edge, the Hamiltonian becomes $H = H_u + H_d + H_{ud}$. The Heisenberg equations of motion $i\hbar\partial_t \hat{A} = [\hat{A}, H]$ for $\hat{\psi}_u(x, t)$ and $\hat{d}(t)$ yield the following set of differential equations

$$\begin{aligned} i\hbar\partial_t \hat{\psi}_u(x, t) &= -i\hbar v_F \partial_x \hat{\psi}_u(x, t) + t_d \hat{d}(t) \delta(x - x_d), \\ i\hbar\partial_t \hat{d}(t) &= \epsilon_d \hat{d}(t) + t_d \hat{\psi}_u(x_d, t). \end{aligned}$$

Fourier transforming the above differential equations, we obtain

$$\epsilon \hat{\psi}_u(x, \epsilon) = -i\hbar v_F \partial_x \hat{\psi}_u(x, \epsilon) + t_d \hat{d}(\epsilon) \delta(x - x_d), \quad (\text{C1})$$

$$\epsilon \hat{d}(\epsilon) = \epsilon_d \hat{d}(\epsilon) + t_d \hat{\psi}_u(x_d, \epsilon). \quad (\text{C2})$$

Integrating both sides of Eq. (C1) from x_d^- to x_d^+ , we obtain

$$-i\hbar v_F [\hat{\psi}_u(x_d^+, \epsilon) - \hat{\psi}_u(x_d^-, \epsilon)] + t_d \hat{d}(\epsilon) = 0. \quad (\text{C3})$$

Using the fact $\hat{\psi}_u(x_d, \epsilon) = [\hat{\psi}_u(x_d^+, \epsilon) + \hat{\psi}_u(x_d^-, \epsilon)]/2$, and solving Eqs. (C2) and (C3) simultaneously, one arrives at

$$\hat{\psi}_u(x_d^+, \epsilon) = \frac{\epsilon - \epsilon_d - i\Gamma}{\epsilon - \epsilon_d + i\Gamma} \hat{\psi}_u(x_d^-, \epsilon), \quad (\text{C4})$$

from which, one extracts the transmission amplitude $\tau_d(\epsilon) = \frac{\epsilon - \epsilon_d - i\Gamma}{\epsilon - \epsilon_d + i\Gamma}$, same as the result in Appendix A 4, thus justifying that the assumption $\theta(0) = 1/2$ is reasonable.

Appendix D: Scattering matrix of the Mach-Zehnder-Fano interferometer

The Fisher-Lee relation[53, 54] expresses the scattering matrix's element in terms of the retarded Green's function, demonstrating the equivalence between the Landauer-Büttiker scattering matrix approach and the Green's function formalism. The propagator G_{pq}^r from q to p is related to the transmission amplitude s_{qp} from lead q to lead p by the formula $s_{qp} = i\hbar\sqrt{v_p v_q} G_{pq}^r$, where

$v_{p/q}$ represents the velocity of carriers in lead p/q . The scattering matrix in the current four-terminal setup is a 4×4 matrix with the structure

$$\hat{s} = \begin{pmatrix} 0 & 0 & s_{S_1 D_1} & 0 \\ 0 & 0 & 0 & s_{S_2 D_2} \\ s_{D_1 S_1} & s_{D_1 S_2} & 0 & 0 \\ s_{D_2 S_1} & s_{D_2 S_2} & 0 & 0 \end{pmatrix}, \quad (\text{D1})$$

where

$$s_{D_1 S_1} = [\sqrt{R_1 R_2} \tau_d(\epsilon) - \sqrt{T_1 T_2} e^{i(2\pi \frac{\Phi}{\Phi_0} + \epsilon \Delta L / \hbar v_F)}] e^{i\epsilon(x-x') / \hbar v_F}, \quad (\text{D2})$$

$$s_{D_2 S_2} = [\sqrt{R_1 R_2} - \sqrt{T_1 T_2} \tau_d(\epsilon) e^{-i(2\pi \frac{\Phi}{\Phi_0} + \epsilon \Delta L / \hbar v_F)}] e^{i\epsilon(x-x') / \hbar v_F}, \quad (\text{D3})$$

$$s_{D_2 S_1} = -i[\sqrt{R_1 T_2} \tau_d(\epsilon) + \sqrt{T_1 R_2} e^{i(2\pi \frac{\Phi}{\Phi_0} + \epsilon \Delta L / \hbar v_F)}] e^{i\epsilon(x-x') / \hbar v_F}, \quad (\text{D4})$$

$$s_{D_1 S_2} = -i[\sqrt{R_1 T_2} + \sqrt{T_1 R_2} \tau_d(\epsilon) e^{-i(2\pi \frac{\Phi}{\Phi_0} + \epsilon \Delta L / \hbar v_F)}] e^{i\epsilon(x-x') / \hbar v_F}, \quad (\text{D5})$$

form a 2×2 unitary scattering matrix, satisfying $|s_{D_1 S_1}|^2 = |s_{D_2 S_2}|^2$, $|s_{D_1 S_2}|^2 = |s_{D_2 S_1}|^2$, $\sum_{p'} s_{pp'}^* s_{qq'} = \delta_{pq}$; and

$$s_{S_1 D_1} = e^{-i\epsilon L_1 / \hbar v_F}, \quad s_{S_2 D_2} = e^{-i\epsilon L_2 / \hbar v_F}, \quad (\text{D6})$$

with L_1 and L_2 being the lengths of two outer paths connecting the source and drain contacts. It is straightforward to check that the scattering matrix Eq. (D1) is unitary. Following the scattering matrix theory of shot noise in multi-terminal mesoscopic conductors[48, 49], the components of the shot noise power tensor are

$$S_{pq} = \frac{e^2}{h} \int d\epsilon \sum_{p' \neq q'} s_{pq'}^* s_{pp'} s_{q'p'}^* s_{qq'} [f_{q'}(1 - f_{p'}) + f_{p'}(1 - f_{q'})], \quad p, p', q, q' = S_1, S_2, D_1, D_2, \quad (\text{D7})$$

where $f_p = \theta(\mu_p - \epsilon)$ is the zero temperature limit of the Fermi-Dirac distribution function in contact p . One can readily check that $S_{S_1 S_1} = S_{S_2 S_2} = 0$, which is consistent with the fact that the electron stream injected from either

source is not fluctuating at zero temperature, and

$$S_{D_1 D_1} = \frac{2e^2}{h} \int_0^{eV} \mathcal{T}_{D_1 S_1}(\epsilon) \mathcal{T}_{D_1 S_2}(\epsilon), \quad (\text{D8})$$

$$S_{D_2 D_2} = \frac{2e^2}{h} \int_0^{eV} \mathcal{T}_{D_2 S_1}(\epsilon) \mathcal{T}_{D_2 S_2}(\epsilon). \quad (\text{D9})$$

The transmission probabilities $\mathcal{T}_{pq} = |s_{pq}|^2$. Using the unitary property of the scattering matrix $\sum_r s_{pr}^* s_{rq} = \delta_{pq}$, the nondiagonal components, $S_{pq}, p \neq q$, can be rewritten as

$$S_{pq} = -\frac{2e^2}{h} \int d\epsilon \sum_{p'} s_{pp'}^\dagger s_{qp'} f_{p'} \sum_{q'} s_{qq'}^\dagger s_{pq'} f_{q'}, \quad (\text{D10})$$

which is always negative due to the anti-bunching effect arising from Pauli exclusion principle[47, 48, 55]. Using $f_p^2 = f_p$, we obtain

$$S_{D_1 D_2} = S_{D_2 D_1} = -\frac{2e^2}{h} \int_0^{eV} \mathcal{T}_{D_1 S_1}(\epsilon) \mathcal{T}_{D_1 S_2}(\epsilon). \quad (\text{D11})$$

These components are related to one another by $S_{D_1 D_1} = S_{D_2 D_2} = -S_{D_1 D_2} = -S_{D_2 D_1}$.

-
- [1] U. Fano, Effects of configuration interaction on intensities and phase shifts, *Phys. Rev.* **124**, 1866 (1961).
 [2] A. E. Miroshnichenko, S. Flach, and Y. S. Kivshar, Fano resonances in nanoscale structures, *Rev. Mod. Phys.* **82**, 2257 (2010).
 [3] M. F. Limonov, M. V. Rybin, A. N. Poddubny, and Y. S. Kivshar, Fano resonances in photonics, *Nature Photonics* **11**, 543 (2017).
 [4] H. Beutler, Über absorptionsserien von argon, krypton

- und xenon zu termen zwischen den beiden ionisierungsgrenzen ${}^2P_3^{2/0}$ und ${}^2P_1^{2/0}$, *Z. Phys. A* **93**, 177 (1935).
 [5] R. K. Adair, C. K. Bockelman, and R. E. Peterson, Experimental Corroboration of the Theory of Neutron Resonance Scattering, *Phys. Rev.* **76**, 308 (1949).
 [6] J. A. Simpson and U. Fano, Classification of resonances in the electron scattering cross section of Ne and He, *Phys. Rev. Lett.* **11**, 158 (1963).
 [7] F. Cerdeira, T. A. Fjeldly, and M. Cardona, Effect of

- free carriers on zone-center vibrational modes in heavily doped p-type Si. II. Optical modes, *Phys. Rev. B* **8**, 4734 (1973).
- [8] J. Feist, F. Capasso, C. Sirtori, K. W. West, and L. N. Pfeiffer, Controlling the sign of quantum interference by tunnelling from quantum wells, *Nature (London)* **390**, 589 (1997).
- [9] V. Madhavan, W. Chen, T. Jamneala, M. F. Crommie, and N. S. Wingreen, Tunneling into a Single Magnetic Atom: Spectroscopic Evidence of the Kondo Resonance, *Science* **280**, 567 (1998).
- [10] J. Göres, D. Goldhaber-Gordon, S. Heemeyer, and M. A. Kastner, Fano resonances in electronic transport through a single-electron transistor, *Phys. Rev. B* **62**, 2188 (2000).
- [11] U. Meirav, M. A. Kastner, and S. J. Wind, Single-electron charging and periodic conductance resonances in GaAs nanostructures, *Phys. Rev. Lett.* **65**, 771 (1990).
- [12] C. W. J. Beenakker, Theory of Coulomb-blockade oscillations in the conductance of a quantum dot, *Phys. Rev. B* **44**, 1646 (1991).
- [13] W. Porod, Z. Shao, and C. S. Lent, Transmission resonances and zeros in quantum waveguides with resonantly coupled cavities, *Appl. Phys. Lett.* **61**, 1350 (1992).
- [14] E. Tekman and F. Bagwell, Fano resonances in quasi-one-dimensional electron waveguides, *Phys. Rev. B* **48**, 2553 (1993).
- [15] Z. Shao, W. Porod, and C. S. Lent, Transmission resonances and zeros in quantum waveguide systems with attached resonators, *Phys. Rev. B* **49**, 7453 (1994).
- [16] J. U. Nöckel and A. Douglas Stone, Resonance line shapes in quasi-one-dimensional scattering, *Phys. Rev. B* **50**, 17415 (1994).
- [17] A. A. Clerk, X. Waintal, and P. W. Brouwer, Fano Resonances as a Probe of Phase Coherence in Quantum Dots, *Phys. Rev. Lett.* **82**, 4636 (2001).
- [18] K. Kobayashi, H. Aikawa, S. Katsumoto, and Y. Iye, Tuning of the Fano effect through a quantum dot in an Aharonov-Bohm interferometer, *Phys. Rev. Lett.* **88**, 256806 (2002).
- [19] K. Kobayashi, H. Aikawa, S. Katsumoto, and Y. Iye, Mesoscopic Fano effect in a quantum dot embedded in an Aharonov-Bohm ring, *Phys. Rev. B* **68**, 235304 (2003).
- [20] A. Aharony, O. E-Wohlman, T. Otsuka, S. katsumoto, H. Aikawa, and K. Kobayashi, Breakdown of phase rigidity and variations of the Fano effect in closed Aharonov-Bohm interferometers, *Phys. Rev. B* **73**, 195329 (2006).
- [21] K. Kobayashi, H. Aikawa, A. Sano, S. Katsumoto, and Y. Iye, Fano resonance in a quantum wire with a side-coupled quantum dot, *Phys. Rev. B* **70**, 035319 (2004).
- [22] A. C. Johnson, C. M. Marcus, M. P. Hanson, and A. C. Gossard, Coulomb-Modified Fano Resonance in a One-Lead Quantum Dot, *Phys. Rev. Lett.* **93**, 106803 (2004).
- [23] A. Fuhrer, P. Brusheim, T. Ihn, M. Sigrist, K. Ensslin, W. Wegscheider, and M. Bichler, Fano effect in a quantum-ring-quantum-dot system with tunable coupling, *Phys. Rev. B* **73**, 205326 (2006).
- [24] B. R. Bulka and P. Stefański, Fano and Kondo Resonance in Electronic Current through Nanodevices, *Phys. Rev. Lett.* **86**, 5128 (2005).
- [25] H. Hofstetter, J. König, and H. Schoeller, Kondo Correlations and the Fano Effect in Closed Aharonov-Bohm Interferometers, *Phys. Rev. Lett.* **87**, 156803 (2005).
- [26] M. E. Torio, K. Hallberg, A. H. Ceccatto, and C. R. Proetto, Kondo resonances and Fano antiresonances in transport through quantum dots, *Phys. Rev. B* **65**, 085302 (2002).
- [27] A. A. Aligia and C.R. Proetto, Kondo and anti-Kondo resonances in transport through nanoscale devices, *Phys. Rev. B* **65**, 165305 (2002).
- [28] M. Sato, H. Aikawa, S. Katsumoto, and Y. Iye, Observation of the Fano-Kondo Antiresonance in a Quantum Wire with a Side-Coupled Quantum Dot, *Phys. Rev. Lett.* **95**, 066801 (2005).
- [29] K. Kang, S. Y. Cho, J. J. Kim, and S. C. Shin, Anti-Kondo resonance in transport through a quantum wire with a side-coupled quantum dot, *Phys. Rev. B* **63**, 113304 (2007).
- [30] Y. Ji, Y. Chung, D. Sprinzak, M. Heiblum, D. Mahalu, and H. Shtrikman, An electronic Mach-Zehnder interferometer, *Nature (London)* **422**, 415 (2003).
- [31] V. S.-W. Chung, P. Samuelsson, and M. Büttiker, Visibility of current and shot noise in electrical Mach-Zehnder and Hanbury Brown Twiss interferometers, *Phys. Rev. B* **72**, 125320 (2005).
- [32] L. V. Litvin, H.-P. Tranitz, W. Wegscheider, and C. Strunk, Decoherence and single electron charging in an electronic Mach-Zehnder interferometer, *Phys. Rev. B* **75**, 033315 (2007).
- [33] I. Neder, F. Marquardt, M. Heiblum, D. Mahalu, and V. Umansky, Controlled dephasing of electrons by non-gaussian shot noise, *Nat. Phys.* **3**, 534 (2007).
- [34] P. Roulleau, F. Portier, D. C. Glattli, P. Roche, A. Cavanna, G. Faini, U. Gensser, and D. Mailly, Finite bias visibility of the electronic Mach-Zehnder interferometer, *Phys. Rev. B* **76**, 161309 (2007).
- [35] E. Sukhorukov and V. Cheianov, Resonant Dephasing in the Electronic Mach-Zehnder Interferometer, *Phys. Rev. Lett.* **99**, 156801 (2007).
- [36] J. T. Chalker, Y. Gefen, and M. Y. Veilleter, Decoherence and interactions in an electronic Mach-Zehnder interferometer, *Phys. Rev. B* **76**, 085320 (2007).
- [37] I. P. Levkivskyi and E. V. Sukhorukov, Dephasing in the electronic Mach-Zehnder interferometer at filling factor $\nu = 2$, *Phys. Rev. B* **78**, 045322 (2008).
- [38] E. Bieri, M. Weiss, O. Göktas, M. Hauser, C. Schönenberger, and S. Oberholzer, Finite-bias visibility dependence in an electronic Mach-Zehnder interferometer, *Phys. Rev. B* **79**, 245324 (2009).
- [39] E. Weisz, H. K. Choi, M. Heiblum, Y. Gefen, V. Umansky, and D. Mahalu, Controlled Dephasing of an Electron Interferometer with a Path Detector at Equilibrium, *Phys. Rev. Lett.* **109**, 250401 (2012).
- [40] I. Neder, M. Heiblum, Y. Levinson, D. Mahalu, and V. Umansky, Unexpected behavior in a two-path interferometer, *Phys. Rev. Lett.* **96**, 016804 (2006).
- [41] H. Le Sueur, C. Altimiras, U. Gennser, A. Cavanna, D. Mailly, and F. Pierre, Energy Relaxation in the Integer Quantum Hall Regime, *Phys. Rev. Lett.* **105**, 056803 (2010).
- [42] S. Tewari, P. Roulleau, C. Grenier, F. Portier, A. Cavanna, U. Gennser, D. Mailly, and P. Roche, Robust quantum coherence above the Fermi sea, *Phys. Rev. B* **93**, 035420 (2016).
- [43] E. G. Idrisov, I. P. Levkivskyi, and E. V. Sukhorukov, Dephasing in a Mach-Zehnder Interferometer by an Ohmic Contact, *Phys. Rev. Lett.* **121**, 026802 (2018).
- [44] E. Buks, R. Schuster, M. Heiblum, D. Mahalu, and V. Umansky, Dephasing in electron interference by a 'which-

- path' detector, *Nature (London)* **391**, 871 (1998).
- [45] D. Sprinzak, E. Buks, M. Heiblum and H. Shtrikman, Controlled Dephasing of Electrons via a Phase Sensitive Detector, *Phys. Rev. Lett.* **84**, 5820 (2000).
- [46] M. Scully and M. S. Zubairy, *Quantum optics* (Cambridge University Press, 1997).
- [47] M. Büttiker, Scattering theory of thermal and excess noise in open conductors, *Phys. Rev. Lett.* **65**, 2901(1990).
- [48] M. Büttiker, Scattering theory of current and intensity noise correlations in conductors and wave guides, *Phys. Rev. B* **46**,12485 (1992).
- [49] Y. M. Blanter and M. Büttiker, Shot noise in mesoscopic conductors, *Phys. Rep.* **336**, 1 (2000).
- [50] Y. Meir, N. S. Wingreen, and P. A. Lee, Transport through a strongly interacting electron system: Theory of periodic conductance oscillations, *Phys. Rev. Lett.* **66**, 3048 (1991).
- [51] H. J. W. Haug, and A-P Jauho, *Quantum kinetics in transport and optics of semiconductors* (Second edition, Springer, 2008).
- [52] A. Houghton, N. Read, H. Won, 1/N expansion for the transport coefficients of the single-impurity Anderson model, *Phys. Rev. B* **35**, 5123 (1987).
- [53] D. S. Fisher and P. A. Lee, Relation between conductivity and transmission matrix, *Phys. Rev. B* **23**, 6851 (1981).
- [54] S. Datta, *Electronic transport in mesoscopic systems* (Cambridge University Press, 2002).
- [55] T. martin and R. landauer, Wave-packet approach to noise in multichannel mesoscopic systems, *Phys. Rev. B* **45**, 1742 (1992).